



HAL
open science

Along-strike segmentation of seismic tremor and its relationship with the hydraulic structure of the subduction fault zone

Gaspard Farge, Claude Jaupart, William Frank, Nikolai Shapiro

► To cite this version:

Gaspard Farge, Claude Jaupart, William Frank, Nikolai Shapiro. Along-strike segmentation of seismic tremor and its relationship with the hydraulic structure of the subduction fault zone. *Journal of Geophysical Research: Solid Earth*, 2023, 128 (12), pp.e2023JB027584. 10.1029/2023JB027584 . hal-04312844

HAL Id: hal-04312844

<https://hal.science/hal-04312844>

Submitted on 28 Nov 2023

HAL is a multi-disciplinary open access archive for the deposit and dissemination of scientific research documents, whether they are published or not. The documents may come from teaching and research institutions in France or abroad, or from public or private research centers.

L'archive ouverte pluridisciplinaire **HAL**, est destinée au dépôt et à la diffusion de documents scientifiques de niveau recherche, publiés ou non, émanant des établissements d'enseignement et de recherche français ou étrangers, des laboratoires publics ou privés.

1 **Along-strike segmentation of seismic tremor and its**
2 **relationship with the hydraulic structure of the**
3 **subduction fault zone**

4 **Gaspard Farge^{1,2*}, Claude Jaupart¹, William B. Frank³ and Nikolai M.**
5 **Shapiro⁴**

6 ¹Université de Paris, Institut de Physique du Globe de Paris, CNRS, F-75005 Paris, France

7 ²Department of Earth and Planetary Sciences, University of California Santa Cruz, Santa Cruz, CA, USA

8 ³Earth, Atmospheric and Planetary Sciences, Massachusetts Institute of Technology, Cambridge, MA, USA

9 ⁴Institut de Sciences de la Terre, Université Grenoble Alpes, CNRS (UMR5275), Grenoble, France

10 **Key Points:**

- 11 • In subduction zones, the intensity of temporal clustering and the periodicity of
12 tectonic tremor are segmented along-strike
13 • We use a model of fluid circulation in the fault to show that segmentation of ac-
14 tivity can be caused by variation of transport properties
15 • Tremor segmentation aligns with subducting seamounts in Shikoku, Japan, sug-
16 gestive of the influence of slab topography

*gafarge@ucsc.edu

Corresponding author: Gaspard Farge, gafarge@ucsc.edu

Abstract

Along the strike of subduction zones, tectonic tremor episodicity is segmented on a geologic scale. Here, we study how this segmentation reflects large-scale variations of the structure and conditions of the fault interface where tremor is generated. We try to understand which properties of the hydraulic system of the fault allow elementary tremor sources to synchronize, leading to the emergence of long-period, large-scale episodic activity. We model tremor sources as being associated with rapid openings of low-permeability valves in the fault zone, which channels the upward flow of metamorphic fluids. Valve openings cause pressure transients that allow interaction between sources. In such a system, tremor activity is thus controlled by unsteady fluid circulation. Using numerical simulations of fluid flow, we explore the impact of valve spatial distribution and fluid flux on the emergence of large-scale patterns of tremor activity. We show that when valves are densely distributed and submitted to near-critical input flux, they synchronize and generate more episodic activity. Based on our model, the most periodic and spatially coherent tremor bursts should thus be emitted from segments densely populated with valves, and therefore of lower permeability than less synchronized segments. The collective activity of their valve population is responsible for fluid-pressure cycling at the subduction scale. In the tremor zone of Shikoku, Japan, the most temporally clustered segment coincides with a downgoing seamount chain, suggesting that the segmentation of the fault zone permeability, and hence of tremor activity, could be inherited from the topography of the subducting oceanic plate.

Plain Language Summary

In subduction, the fault zone controls plate convergence through friction, controlling if, when and where earthquakes occur. At depths larger than about 40 km, deformation in the fault vicinity transitions to a more stable, ductile regime. At those depths, no earthquakes are expected, and noisy, emergent tectonic tremor are detected instead. Geological and geophysical observations link tremor with the unsteady circulation of high-pressure fluid in the fault zone. Tremor could thus help understand how fluid flows along the subduction interface, where it acts to lower the fault strength and may therefore trigger seismic events. Tremor occurs intermittently, in bursts followed by quiet periods. In this study, we investigate the role of fluid circulation processes in generating tremor, and why its activity varies across different regions. In our model, the intermittence of tremor comes from the intermittence of fluid circulation in the fault. We describe how many small parts of the fault zone can interact, and open or close coherently, generating pulses of fluid flow and the observed bursts of tremor. This framework allows to interpret variations of tremor intermittence as a symptom of how strong the flow and how well fluid circulates in different parts of the subduction interface.

1 Introduction**1.1 Source processes of tectonic tremor and low-frequency earthquakes**

In the deeper parts of subduction faults (at about 40 km depth), seismic signals with a lower frequency than earthquakes are detected in a wide frequency band ranging from 0.01 Hz to 10 Hz. Impulsive events called *low-frequency earthquakes* (LFEs) and *very-low frequency earthquakes* (VLFEs) are detected in narrow high (1–10 Hz) and low (0.02–0.05 Hz) frequency bands, respectively (Obara, 2002; Katsumata & Kamaya, 2003; Ito et al., 2007). *Tectonic tremor* is a long (10s to days), emergent seismic signal in which LFEs and VLFEs are almost systematically detected, from the same localized sources, which persist through time (Rubin & Armbruster, 2013; Chestler & Creager, 2017). Tremor, LFEs and VLFEs appear to be systematically correlated with one another in space and time, suggesting that they are manifestations of the same broadband phenomenon in different frequency intervals (*e.g.* Masuda et al., 2020). In this study, we will study the

collective, long-term patterns of LFE activity to understand their underlying physical processes. We will therefore use the terms “tremor” or “tremor activity” as a synonym for LFE activity, considering that tremor is composed of many LFEs (Shelly et al., 2006; Ide, 2021) — although we recognize that this approach might gloss over potentially different source processes. Tremor activity is intermittent and proceeds in periods of intense activity formed of clusters of LFEs, separated by periods of quiescence (Obara, 2002; Rogers, 2003; Shelly et al., 2007; Brudzinski et al., 2010; Frank et al., 2014; Idehara et al., 2014). The temporal clustering of activity, the duration, sizes and recurrence timescales of tremor bursts vary between subduction zones. Bursts typically last from less than an hour to a week and are separated by hours to months (*e.g.* Frank et al., 2014). Thus, the timescales of tectonic tremor activity can be several orders of magnitude longer than the average recurrence time and duration on an individual LFE.

The geological processes that generate tectonic tremor remain elusive. The strongest episodes of tremor occur during slow-slip events on the fault interface (Obara et al., 2004; Rogers, 2003; Shelly et al., 2006; Frank, Radiguet, et al., 2015) and episodes of strong fluid pressure variations in their source region (Frank, Shapiro, et al., 2015; Nakajima & Uchida, 2018; Tanaka et al., 2018; Warren-Smith et al., 2019; Gosselin et al., 2020). This hints at recurring cycles of accumulation and release of hydro-mechanical stress in the fault often called *fault-valving* R. Sibson (1992). As fluid is released through metamorphic dehydration reactions of the oceanic crust (Anderson et al., 1976), regions of low permeability above the slab can seal the interface, leading to high-pressure anomalies (Shelly et al., 2006; Calvert et al., 2011; Wannamaker et al., 2014). These lead to decreased effective normal stress on the fault, and slip can therefore nucleate with minor changes of the stress field. As the slip front propagates, fueled and stabilized by the high fluid pressures (Segall et al., 2010), the induced fracturing is likely to open fluid pathways, thereby lowering the local fluid pressure (Frank, Shapiro, et al., 2015). Strong tremor activity seems to occur during this phase. When the permeability around the fault heals, fluid pressure rises again, and a new cycle begins (R. Sibson, 1992).

The geological study of outcrops of paleo-subduction zones indicates that fluid pressures are indeed highly heterogeneous and variable, with evidence of supra-lithostatic pressures triggering vein-opening (Angiboust et al., 2015; Muñoz-Montecinos et al., 2021; Taetz et al., 2018; Tarling et al., 2021; Platt et al., 2018; Behr & Bürgmann, 2021). The radiation patterns of LFEs, VLFs and tremor is at least in part consistent with shear slip along the fault interface (Ide et al., 2007; Royer & Bostock, 2014; Ide & Yabe, 2014; Imanishi et al., 2016), triggered by aseismic slow slip (Ando et al., 2010; Ben-Zion, 2012; Sammis & Bostock, 2021). The accumulation of geologic evidence of coupled deformation and fluid flow at the source scale suggests that LFEs are also possibly associated with fluid movement in the fault (Muñoz-Montecinos et al., 2021; Taetz et al., 2018). The sudden fluid mass advection could generate a single-force source on the matrix (Takei & Kumazawa, 1994), producing an LFE wavefield with a radiation pattern hardly distinguishable from a double-couple owing to the small aperture of seismic networks in subduction zones (Shapiro et al., 2018; Ohmi & Obara, 2002). A similar model has been suggested by Ukawa and Ohtake (1987) to explain low frequency volcanic earthquakes that may be generated by a sudden acceleration of fluid that would result in a changing viscous shear force acting on the conduit walls and oriented parallel to the flow. In this hydraulic process, the LFE source duration is controlled solely by the fluid diffusivity of the permeable medium, and does not depend on event magnitude, which is consistent with observations in Cascadia and Guerrero, Mexico (Bostock et al., 2015; Farge et al., 2020). This key property does not hold in Japanese subduction zones, however, which led some authors to attribute it to an observational bias (Ide, 2019; Supino et al., 2020).

The very small magnitude of LFEs and restrictions on the number of seismic stations that can hamper a clear-cut diagnosis of LFE source mechanisms. Thus, we take a different approach and focus on the role fluid flow processes. In the R. Sibson (1992)

120 valve mechanism, fault slip and changes of fluid pressure are coupled. The common as-
 121 sumption is that abrupt pressure changes are triggered by seismic rupture but we shall
 122 argue that they could well be due to processes internal to the permeable fault zone. One
 123 key feature of LFE activity is that tremor bursts involve seismic sources of limited ex-
 124 tent (hundreds of meters at most) and take place over large distances (tens of kilome-
 125 ters), showing that some long-range interaction mechanism is at work. This has usually
 126 been attributed to slow-slip propagation but simple models of tremor and seismicity show
 127 that fluid-assisted interaction between neighbouring sources can also lead to long-range
 128 synchronization (Farge et al., 2021; Fukuda et al., 2022). The smallest patterns of LFE
 129 clustering last less than an hour, which is consistent with source-scale processes.

130 **1.2 Segmentation of tremor intermittence in subduction zones**

131 Tremor activity is segmented in subduction zones: the recurrence intervals and tem-
 132 poral clustering are variable along both the dip and strike of the fault. In many subduc-
 133 tion zones, tremor activity is not evenly distributed and several segments with different
 134 time clustering characteristics can be delimited along the strike of the fault (Poiata, Vilotte,
 135 Shapiro, Supino, & Obara, 2021; T. Wang et al., 2018; Brudzinski & Allen, 2007; Husker
 136 et al., 2019). The geologic scale (tens to hundreds of kilometers) and permanence of such
 137 segmentation indicates that it is likely due to large-scale, structural heterogeneity in the
 138 fault zone (Brudzinski & Allen, 2007; Maury et al., 2018; Ide, 2010). Spatial variations
 139 of frictional stress and weakness are likely to shape both the source-scale distribution
 140 of tremor sources, and the large-scale segmentation of tremor episodicity (Nakajima &
 141 Hasegawa, 2016; Kano et al., 2018; Cattania & Segall, 2021). The local plate dehydra-
 142 tion rate, magnitude of fluid escape away from the fault zone, and thus the local fluid
 143 pressure and flow conditions are also bound to control the source- and regional-scale dis-
 144 tribution of tremor (Audet & Bürgmann, 2014; Halpaap et al., 2019; Gosselin et al., 2020;
 145 McLellan et al., 2022). One can anticipate that the characteristics of segment-scale ac-
 146 tivity are rooted in the spatial distribution of seismic sources (shorter-scale heterogene-
 147 ity), which has been shown to be a stationary structural feature of the plate interface (Rubin
 148 & Armbruster, 2013). If fluid circulation is a major control mechanism, however, the flow
 149 rate is also likely to be a key variable.

150 The tremor zone in Shikoku in the Nankai subduction zone (Japan) is particularly
 151 well suited for studying the structure of the fault interface at tremor depths. Long-term,
 152 high-resolution catalogs of tremor and LFE in this region reveal large-scale spatial struc-
 153 tures on the subduction interface (Ide, 2010). They allow to resolve a temporal cluster-
 154 ing and tremor burst recurrence at subdaily timescales, and their segmentation along
 155 the fault (T. Wang et al., 2018; Poiata, Vilotte, Shapiro, Supino, & Obara, 2021; Ide &
 156 Nomura, 2022). Studies have attributed the segmentation of temporal activity to regional
 157 scale variations in frictional strength of the megathrust, due to locally drained or undrained
 158 conditions in the interface (Kano et al., 2018; Nakajima & Hasegawa, 2016). In a pre-
 159 vious study (Farge et al., 2021), we have designed a model suitable to investigate in more
 160 details how dynamic fluid circulation processes could shape tremor activity in this re-
 161 gion. By modeling source distribution and interactions in the fault, it allows us to link
 162 temporal characteristics of seismicity to the dynamic of fluid circulation in the fault, and
 163 its structural controls.

164 In this study, our aim is therefore to understand how the temporal patterns of tremor
 165 activity in Shikoku can provide an information about the local structure of hydraulic con-
 166 ditions in the fault zone. To do so, we will investigate how tremor sources can synchro-
 167 nize, and how they conspire to shape the observed temporal clustering of activity, long
 168 recurrence timescales, and coherence of activity over wide spatial scales. We focus our
 169 analysis on the role of the dynamics of permeability, fluid flux and fluid pressure in the
 170 fault zone. We build upon an earlier study of along-dip fluid circulation in a dynami-
 171 cally permeable fault zone, where low-permeability plugs open and close in a valve-like

manner (Farge et al., 2021). The valve mechanism simulates local changes of permeability and fluid pressure that may be associated with LFE source processes. We have previously shown that in such a system, realistic, tremor-like patterns of activity emerge due to the dynamics of fluid pressure. In the present work, we systematically explore how the hydraulic forcing (the input fluid flux) and the spatial distribution of low-permeability valves control the intermittence of seismicity, and how in turn, the temporal characteristics of activity can be used to infer the hydraulic conditions in the fault interface.

The article is organized as follows. (1) We describe a new method to characterize the temporal clustering and recurrence timescales of LFE activity. We apply this method to characterize the segmentation of tremor intermittence in Shikoku, Japan. (2) We summarize key aspects of the valve model and the hydraulic and seismic behavior it produces. (3) We explore the interaction between two permeability valves. We show that its strength is controlled by the input fluid rate as well as the valve separation. (4) In a fourth part, we systematically explore how the spatial distribution of valves — their number and spatial clustering — and the input flow rate set the intermittence of tremor activity. Using simulations to explore the flux/valve distribution phase space, we explore how they determine the strength of long-range interactions, and hence control how synchronized the activity is. (5) In a last part, we elaborate on the physical origin of tremor activity segmentation in the Shikoku (Japan) subduction zone. We end the paper with a discussion of the scope and limitations of our model.

2 Characterizing tremor intermittence

2.1 Clustering and characteristic timescales of LFE activity

Tremor activity can be described in two complementary ways: either through a continuous prism by measuring how long or how often a tremor source is active in time, or through a more discrete *point process* description, looking at the occurrences of individual events, LFEs. In a point process description of the activity, LFEs occur in a “bursty” manner, with very short and very long inter-event delays much more probable than in a constant-rate, Poisson process (Goh & Barabasi, 2006). They form *clusters* of rapid LFE occurrences (sub-hourly delays), separated by long, quiet periods (one event per day or less) (Frank et al., 2014). LFE clusters — *i.e.* tremor bursts — last between an hour and a week. Similarly to LFEs, their occurrences cluster in time, more likely occurring soon before or after another burst. The degree of temporal clustering of activity varies between subduction zones, and between segments of a subduction zone. Some zones can exhibit an extremely clustered activity in time, with almost no background seismicity, and larger, less frequent bursts dominating the activity, while other regions can produce less clustered, more continuous activity, formed of smaller, shorter, more frequent bursts. Single bursts of activity can be spaced by a few hours in the most active periods, which recur on the scale of months to years. This superimposition of timescales of recurrence — individual events, clusters, clusters of clusters, etc — is characterized as a “scale-free” phenomenon by studies on tremor (Idehara et al., 2014) and LFE activity (Frank et al., 2016; Poiata, Vilotte, Shapiro, Supino, & Obara, 2021). However, when looking at the largest bursts of activity in a given region, one or several characteristic timescales of recurrence can be estimated. In the tremor zone of Guerrero (Mexico) for instance, the largest tremor bursts, associated with large (geodetic magnitude M7.5) slow-slip events recur every 4 to 5 years (Radiguet et al., 2012). Smaller bursts occur every three months or so, activating smaller parts of the fault, associated with M6.4 slow-slip events (Frank, Radiguet, et al., 2015; Frank & Brodsky, 2019). Ide and Nomura (2022) proposed a systematic characterisation of long-term and short-term recurrence of tremor episodes in the Nankai subduction zone, highlighting periods of 10–100 days and 1–10 hours. It is likely that the period of recurrence of tremor bursts reflects characteristic spatial scales of the dynamics at play: while the shorter period might reflect

source-to-source local interactions, the longest detectable periods could be caused by large-scale synchronization of whole segments of the subduction interface.

2.2 The segmentation of LFE activity in Shikoku

In Figure 1e, we represent the LFE activity in time along the strike of the Shikoku tremor zone, in Japan (catalog from Poiata, Vilotte, Shapiro, Supino, & Obara, 2021). Three zones with different clustering and recurrence behavior can be visually identified, from least to most temporally clustered: zone 1, the westernmost part between 50–140 km along strike, zone 2, the easternmost part between 190–250 km along strike, and zone 3 in between, 140–190 km. In zone 1, activity is characterized by a relatively low level of temporal clustering, and a high background rate of events. Bursts are frequent, and recur on timescales of 2–3 months, although with a strong variability. In the easternmost zone, activity is more clustered, and bursts are slightly less frequent, recurring every 3 months in the eastern and western halves of the zone. Finally, in the boundary region between the two previous zones, the activity is least intense, with a very low background rate. Most of the events occur during large transients of activity starting in neighboring segments which propagate into the middle one, every 6 months to slightly less than a year. It is the most temporally clustered activity of the three regions. In other subduction zones, similar variations of temporal clustering and recurrence timescales can be observed, showing a clear along-strike segmentation of tremor activity. In the supplementary materials, we show time series of tremor activity rate in the Central American subduction zone (Figures S1, tremor catalog from Husker et al. (2019)) and along the Cascadia subduction zone (Figure S2, tremor catalog from Wech (2021)). In Shikoku, Guerrero, and Cascadia, the segments are of geological scale, spanning tens to hundreds of kilometers along the strike of the subduction.

In all examples presented here (Shikoku in Figure 1, Guerrero in Figure S1 and Cascadia in Figure S2), the variations of temporal clustering, regularity of the recurrence and timescale of recurrence seem to be correlated: the stronger the clustering, the longer and more regular the recurrence, and therefore the more periodic the activity. In the light of this, large clusters, quasi-periodic behavior and long recurrence intervals can be interpreted as effects of the *synchronization* of the activity of tremor sources through physical interactions between them. Given a constant rate of activity for many sources, the stronger the synchronization between them, the more likely events are to occur within clusters, the larger the clusters, and therefore the longer their recurrence times. Measuring synchronization through temporal clustering and the timescale and regularity of the recurrence of activity therefore provides important insight into the physical mechanisms that allow tremor sources to interact, and shape their collective behavior.

2.3 Clustering and recurrence analysis

In order to study the synchronization of LFEs in models and observations, we design simple measures of the level of clustering of activity, and of timescales of recurrence of clusters of activity, and how variable they are. Because we want to capture the larger-scale dynamics of tremor generating processes, those measures are designed to capture the longer periods of tremor episodicity. They are based on an explicit detection of clusters, to avoid the ambiguity of spectral measurements — based on autocorrelation or Fourier analysis of activity time series for instance (*e.g.* Beaucé et al., 2019) — regarding which specific patterns the measured timescales are related to. The measures and algorithm are designed to be used automatically and with minimal tuning on both real and simulated catalogs of events, with a focus on being able to characterize both relatively constant and very clustered activity. This will allow us to gain a direct understanding of the characteristics of synthetic seismicity for large batches of simulations (several tens of thousands), with no changes of parameters.

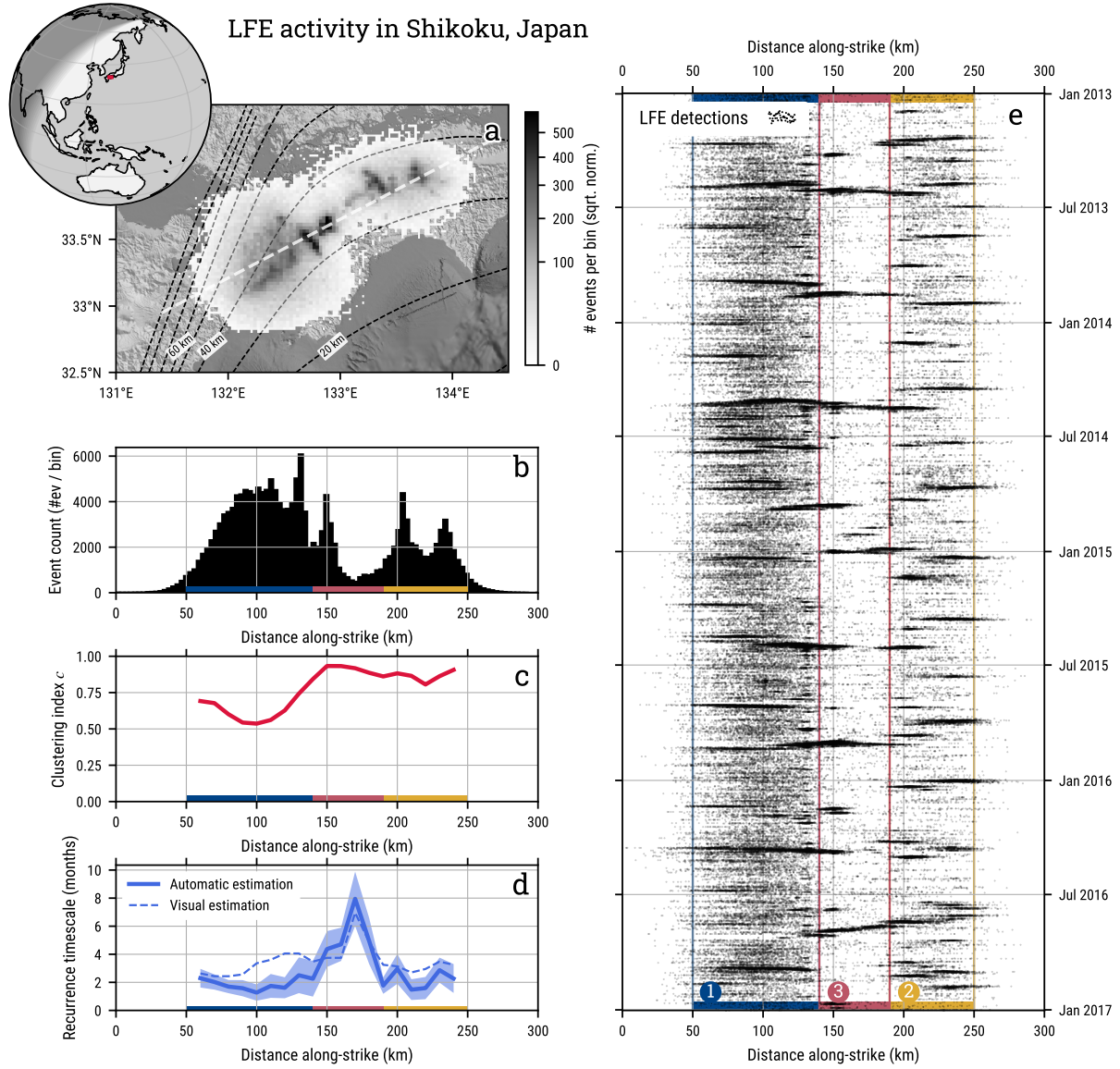


Figure 1: Caption on next page.

Figure 1. *On previous page.* Patterns of temporal clustering and recurrence of LFE activity, in Shikoku, Japan (2013–2017). (a) 2D histogram of LFE activity in 2.7 km by 2.7 km horizontal bins, colored according to the number of sources projected onto the surface (catalog from Poiata, Vilotte, Shapiro, Supino, and Obara (2021)). Depth contours of the slab are taken from a model by Iwasaki et al. (2015). The dotted white line indicates the along-strike direction. (b) Event count binned in 3-km wide bins along-strike, for the full period. (c) Intensity of temporal clustering along-strike, measured by the clustering index c in bins of 20 km, with a 10 km overlap. (d) Recurrence timescale of clusters along strike, with the same spatial bins as in (c). Details on the cluster detection and clustering index can be found in Section 2.3. The blue, shaded area around the measurement represents 1- σ interval around the estimated recurrence timescale. A visually estimated recurrence is shown as a dotted blue line. (e) LFE activity along-strike in time, each black dot represents an event. Three major segments are highlighted in blue (zone 1), yellow (zone 2) and red (zone 3). See text for details, and Figure 12 for wider geographical context.

273 The first measure is a temporal clustering index c , which quantifies the extent to
 274 which events occur within clusters, rather than as a more homogeneous process in time.
 275 To do so, we measure the proportion p_{ev}^{peaks} of events occurring during “peaks” in the
 276 time series of event counts — the number of events per time bin δt . For later reference,
 277 we chose $\delta t = 3e - 4$ to count events produced in our simulations, and $\delta t = 2$ days to
 278 count events in observed tremor in Shikoku (Figure 1). Peaks of activity are defined as
 279 all consecutive bins in which the event count is higher than 66% of the time — follow-
 280 ing a similar methodology as Frank, Shapiro, et al. (2015) for LFE burst detection. Peaks
 281 therefore cover about 34% of the time period. For a constant activity rate (for instance
 282 a Poisson process), events are homogeneously distributed in time, thus about 34% of the
 283 events occur during peaks. If the activity is clustered, events occur mostly during peaks,
 284 and p_{ev}^{peaks} is higher than 34%. The clustering index c is constructed by mapping linearly
 285 the proportion of events in peaks p_{ev}^{peaks} to 0–1:

$$c = \frac{p_{ev}^{peaks} - 0.34}{1 - 0.34} \quad (1)$$

286 If 100% of events are in peaks, events occur only in clusters and $c = 1$. If only 34% of
 287 events occur in peaks, events are more or less as likely to occur in peaks as outside of
 288 peaks, the activity is not clustered and $c = 0$. Figure S4 and Section 2 of the supple-
 289 mentary materials illustrate and describe this step of the analysis in more details.

290 In a second step, we measure the characteristic timescales of recurrence and their
 291 regularity. We perform this analysis only if the activity is temporally clustered, when
 292 $c > 0.25$ — *i.e.* more than 50% of events are in peaks. To do so, we design an auto-
 293 matic identification of clusters of events in time, based on the proximity of their occur-
 294 rence times t_i . Clusters of events are detected using a density-based clustering algorithm
 295 (DBSCAN, (Ester et al., 1996), *scikit-learn* implementation (Pedregosa et al., 2011), choice
 296 of parameters is detailed in Section S2.3 of the Supporting Information). Clusters of events
 297 are then classified according to the number of events that make them up, using DBSCAN
 298 on cluster population size. In some cases, more than one characteristic size of clusters
 299 can be detected, and recurrence timescales should be measured only for a given size of
 300 cluster. Measuring the average of inter-cluster time intervals can give an estimation of
 301 the characteristic timescale of recurrence for a given class of clusters, and the ratio of
 302 the standard deviation to the average of inter-cluster times gives an estimate of how vari-
 303 able or regular the recurrence is.

304 By explicitly detecting clusters, and classifying them by size, we implicitly assume
 305 that the clustering of activity exhibits characteristic scales of cluster size, duration or

306 recurrence delay, which is not always the case for LFE activity (Idehara et al., 2014; Frank
 307 et al., 2016; Poiata, Vilotte, Shapiro, Supino, & Obara, 2021), or intermittent microseis-
 308 mic activity in general (Beaucé et al., 2019, 2022), where scale-free behavior is often ob-
 309 served. The algorithm is tailored to focus on the longest timescales of recurrence, that
 310 is on the largest clusters of activity detected in a time series. This timescale is in itself
 311 a characteristic scale of the system, and it is likely controlled of by large-scale structure
 312 of the interface.

313 We apply this method to the activity in Shikoku, to compute the clustering index
 314 c (Figure 1c), the recurrence timescale and its variability (Figure 1d). The automatic
 315 measurements are performed for the whole period (2013–2017), in bins of 20 km along
 316 strike, with 10 km overlap. The segmentation in three zones that we established visu-
 317 ally using the time-dip representation of activity (Figure 1e) is confirmed by the auto-
 318 matic measurements: zone 1 produces the least clustered activity ($c \approx 0.6$), with the
 319 most frequent bursts (about every 2 months), zone 2 produces slightly less frequent bursts
 320 (about every 3 months), and an activity that is overall more clustered ($c \approx 0.8$), and
 321 zone 3 (140–190 km) produces the most clustered activity ($c \approx 0.9$), with the longest
 322 timescales of recurrence (around 6 months). This novel method therefore produces accu-
 323 rate and simple measures of intermittency of real patterns of seismicity, and its effi-
 324 ciency will be most useful to characterize synthetic activity for large batches of simula-
 325 tions, later in this study.

326 3 Model description

327 3.1 A valve model to describe fault zone permeability

328 Many geophysical measurements (*e.g.* Peacock et al., 2011; Audet & Kim, 2016;
 329 Wannamaker et al., 2014; Rubinstein et al., 2009) reveal that the regions of the fault zone
 330 where tremor originates has a high porosity and is saturated with fluid at near-lithostatic
 331 pressures. The fluid is mainly composed of supercritical water, freed from local dehy-
 332 dration reactions of the oceanic plate minerals (Tarling et al., 2019), or originating from
 333 deeper sources and then channeled along the fault zone to the tremor source region (Hyndman
 334 et al., 2015; Taetz et al., 2018). The permeability of the fault zone is characterized by
 335 a higher permeability than the overriding plate, and a strong planar anisotropy, because
 336 of the development of a fabric in the shear zone (Evans et al., 1997; Audet & Kim, 2016).
 337 This permeability structure traps fluid and channels it along the plate interface, pref-
 338 erentially through localized channels of high permeability (Piccoli et al., 2021; Eymold
 339 et al., 2021; Angiboust et al., 2014; Ague, 2014). Updip of the tremor source region, fluid
 340 can partly escape the plate interface through fracture networks in the overriding plate,
 341 or at the root of the accretionary wedge (Hyndman et al., 2015), allowing the pressure
 342 to drop slightly from lithostatic levels. As thoroughly detailed in Farge et al. (2021), Sec-
 343 tion 3, we describe fluid circulation processes in a one-dimensional, high-permeability
 344 channel along the dip of the fault zone, saturated with high-pressure fluid. This chan-
 345 nel is fed at its deep end by a constant metamorphic fluid flux q_{in} , and is bound by a
 346 constant fluid pressure at its outer end, where it outputs to a highly connected fracture
 347 network towards the surface. We represent this system in Figure 2a and b. In a fluid-
 348 saturated porous medium, Darcy’s law dictates that the mass flux of fluid per unit area
 349 of channel cross-section $q(x, t)$ is proportional to the local gradient of fluid pressure $p(x, t)$
 350 along dip, and to permeability $k(x, t)$:

$$q(x, t) = -k(x, t) \times \frac{\rho\phi}{\eta} \times \frac{\partial p}{\partial x}(x, t) \quad (2)$$

351 where η is the fluid viscosity, ρ the fluid’s density, ϕ the fault zone porosity. The fluid
 352 pressure $p(x, t)$ evolves along the dip of the channel x in time t according to a diffusion

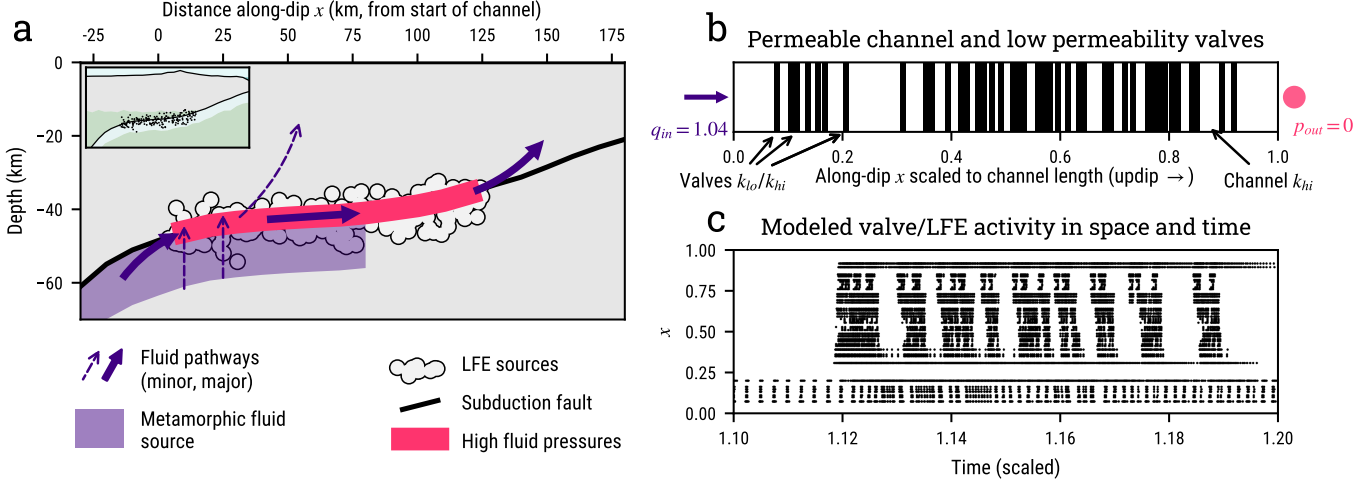


Figure 2. (a) Conceptual representation of fluid circulation in the fault zone. Downdip and below the tremor source region, metamorphic dehydration reactions release fluid, which is channeled in the permeable subduction interface, circulating at high fluid pressures. (b) Schematic representation of the model set up: a 1D permeable channel in which identical valves are distributed (black bars), opening and closing in response to the fluid pressure field. The channel is fed at its base by input fluid flux q_{in} , which is the main control parameter of the experiment. At its top, the channel is connected to a high permeability region such that the fluid pressure is close to the hydrostatic pressure $p_{out} = 0$ (see text for details on the scaling of physical properties). (c) Each valve opening is associated with a seismic event, a model LFE. The activity is represented in a space-time graph, with time on the x -axis, and distance along the channel on the y -axis. Figure reproduced and modified from Farge et al. (2021).

353 equation:

$$\frac{\partial p}{\partial t} = \frac{\partial}{\partial x} \left(D(x, t) \frac{\partial p}{\partial x} \right) \quad (3)$$

354 with a diffusivity

$$D(x, t) = \frac{k(x, t)}{\eta\beta\phi}, \quad (4)$$

355 where β is a composite, fluid-matrix compressibility.

356 In the tremor source region, the combination of a constant fluid input and low-permeability
 357 seal over the fault zone creates the near-lithostatic fluid pressure. Along the fault-zone
 358 channel, permeable segments filled with high pressure fluid are separated by imperme-
 359 able barriers, caused by the fault-zone heterogeneity — for instance in grain/block size,
 360 fracture density and/or thickness of the permeable zone. At equilibrium, the heteroge-
 361 neous distribution of permeability results in a decrease of fluid pressure in a stepwise fash-
 362 ion towards the surface along the dip of the fault : hydrostatic fluid pockets separated
 363 by fluid pressure discontinuities across barriers (Gold & Soter, 1985; Shapiro et al., 2018).
 364 Because the input fluid flux in the fault zone is a constant stressing rate, the fluid pres-
 365 sure can progressively overcome the lithostatic burden just downdip of permeability bar-
 366 riers, forcing the dynamic increase of permeability (Hubbert & Willis, 1957; Etheridge
 367 et al., 1984; R. H. Sibson, 2017), and the fluid influx and rapid fluid pressure adjustment
 368 observed with both geophysical and geological means, at the source (Muñoz-Montecinos
 369 et al., 2021; Taetz et al., 2018) and subduction scale (Angiboust et al., 2015; Warren-
 370 Smith et al., 2019; Gosselin et al., 2020; Nakajima & Uchida, 2018; Tanaka et al., 2018).

371 The dynamic opening of permeability could occur because of various mechanisms: hy-
 372 draulic fracturing caused by the pressure difference across a barrier generating a force
 373 overcoming the rock’s cohesive strength, opening of tensile cracks as fluid pressure over-
 374 comes the lithostatic burden (Hubbert & Willis, 1957), or dilatant slip triggered by the
 375 reduced effective normal stress on friction surfaces (Mitchell & Faulkner, 2008). After
 376 a rapid opening of permeability and relaxation of the fluid pressure, the permeability heals
 377 shut through a combination of clogging by cataclastic grains carried in the fluid (Candela
 378 et al., 2014), and mechanical and chemical cementation of fractures (*e.g.* Yasuhara &
 379 Elsworth, 2008). At the P-T conditions of the tremor source region, hot-pressing exper-
 380 iments suggest that even chemical healing could occur on the scale of days or less (*e.g.*
 381 Giger et al., 2007).

382 In our model, the small-scale heterogeneity of permeability in the channel is rep-
 383 resented in a discrete, binary manner: short segments of the channel have a lower per-
 384 meability k_{lo} than the surrounding $k_{hi} = \lambda k_{lo}$ ($\lambda \gg 1$), as represented in Figure 2b.
 385 The low-permeability segments behave as *valves*. We represent the opening of those seg-
 386 ments in a simple manner: when the pressure difference δp across them exceeds a thresh-
 387 old δp_c^{break} , they instantly change to an open state, and their permeability switches to
 388 k_{hi} . When the accumulated overpressure across a now-open valve diffuses and δp drops
 389 below a lower threshold δp_c^{clog} , the valve then closes instantly, and the permeability in
 390 the segment goes back to k_{lo} . We do not model in details the dynamics either of the open-
 391 ing or closing of permeability. Although simply parameterized, they are based on a con-
 392 sistent modeling of how porous media clogs and unclogs in response to flux, pressure gra-
 393 dient and pore sizes when a particle-laden fluid circulates in it (Jäger et al., 2017; Bianchi
 394 et al., 2018; Souzy et al., 2020; Candela et al., 2014). More details on the modeling and
 395 its consistency can be found in Farge et al. (2021).

396 A key aspect of the model is that the along-dip width of the valve w_v is chosen ar-
 397 bitrarily, as the smallest scale of permeability heterogeneity we describe. Indeed, valves
 398 are elementary, dynamic segments of permeability, and we have shown in a previous study
 399 that their interactions seem to be creating *macro-valves*: segments of the channel of larger
 400 width, with a similar valving behavior (Farge et al., 2021). Here, our goal is to under-
 401 stand what controls this phenomenon, and how it affects the characteristics of seismic
 402 activity in the fault zone. The valves we use should therefore be thin enough that the
 403 effects on the seismicity are dominated by their collective behavior. Their width is set
 404 at a hundredth of the channel length along-dip, to be convenient for our numerical ap-
 405 proach. In essence, each elementary valve can however be composed of many smaller valv-
 406 ing segments, resulting in a macro-valve of scale w_v .

407 In the model, permeability k changes occur without changes in porosity ϕ , which
 408 can occur if changes occur mostly to pore throats, changing the connectivity between
 409 pores (Steinwinder & Beekingham, 2019). Permeability is therefore the only control on
 410 fault zone transport properties in our model. All physical variables are scaled to char-
 411 acteristic values for our system: $x = 1$ is the length of the channel, $k = 1$ is the open
 412 permeability of the channel, $t = 1$ is the diffusive timescale across the channel when
 413 it is fully open, a unit of fluid pressure p corresponds to the lithostatic burden over the
 414 depth of the channel, a unit of fluid q corresponds to the flux obtained when a fluid pres-
 415 sure difference $\Delta p = p(x = 0) - p(x = 1) = 1$ is applied across the full length of the
 416 channel, when its permeability is $k = 1$ everywhere.

417 We assume that each valve opening is associated with an elementary tremor event,
 418 *i.e.* an LFE, emitted from the position of the valve, at the time of opening. It simulates
 419 the opening of permeability that is presumably associated with an LFE triggered by locally-
 420 high fluid pressure, through a rupture, unclogging, or hydrofracture-like event (*e.g.* Ko-
 421 towski & Behr, 2019; Shapiro et al., 2018; Muñoz-Montecinos et al., 2021). The cumu-
 422 lated activity of those synthetic LFEs could build up into signals that could be detected
 423 as large magnitude LFEs, VLFs, and tremor. This description is simplistic, but our fo-

424 cus is not on an accurate physical description of the source of LFEs, VLFs or tremor,
 425 but rather on the sensitivity to and effect on the fluid pressure field of elementary tremor
 426 sources, that allows source-to-source interaction.

427 In practice, we built and optimized a stable, accurate algorithm to solve the dif-
 428 fusion equation, compute fluid flux, valve state and therefore permeability throughout
 429 the channel (Farge et al., 2021). The main control parameters of this system are the value
 430 of the input fluid flux q_{in} , and the valve distribution in the channel. We retrieve a cat-
 431 alog of valve openings, which we consider to be an analog of LFE catalogs. Figure 2c dis-
 432 plays the activity in time and space emitted by valves in a channel, as fluid is forced through
 433 it. To our knowledge, this model is the first to explicitly and causally describe the link
 434 between the hydraulic dynamics in the fault zone and the activity of tremor in time and
 435 space, opening a rich scope of exploration.

436 3.2 Valve behavior for different values of the input flux

437 Closed valves act as barriers to fluid flow in the channel, and as they impede the
 438 flow in the channel, the pressure difference across them can increase to the point they
 439 break. However, the fluid input rate q_{in} into the system controls if a valve can open when
 440 closed, and close when open. Two threshold flux values can be derived from the δp thresh-
 441 olds, using Darcy’s law for the flux through a valve in a permanent regime. The flux needed
 442 to reach the breaking threshold δp_c^{break} when a valve is closed is:

$$q_c^{break} = \frac{\rho}{\eta} k_{lo} \frac{\delta p_c^{break}}{w_v}, \quad (5)$$

443 where w_v is the valve’s width. Therefore, when $q_{in} > q_c^{break}$, δp across a closed valve
 444 will eventually go over δp_c^{break} , and the valve will open. As the valve opens, the steep
 445 pressure gradients diffuses and δp drops across the valve. For the valve to close back, the
 446 strength of the flux has to allow δp to drop below the closing threshold δp_c^{clog} , and there-
 447 fore q_{in} has to be lower than:

$$q_c^{clog} = \frac{\rho}{\eta} k_{hi} \frac{\delta p_c^{clog}}{w_v}. \quad (6)$$

448 In the previous equations, δp_c^{break} and δp_c^{clog} are defined as the difference of pressure from
 449 down- to up dip of the valve, hence a different sign convention than equation 2. It is in-
 450 tuitive that $\delta p_c^{break} > \delta p_c^{clog}$. However, we show in Farge et al. (2021) (Section 4.1) that
 451 because both tortuosity and pore aperture change when pores open, the change of per-
 452 meability is more important than the ratio of the δp threshold, which only depends on
 453 pore aperture, therefore $k_{hi}/k_{lo} > \delta p_c^{break}/\delta p_c^{clog}$ and $q_c^{break} < q_c^{clog}$. In this case, val-
 454 ues of flux determine three distinct valve behaviors:

- 455 • When $q_{in} < q_c^{break}$, the flux is lower than the breaking threshold, and valves will
 456 stay closed, or close if they are open.
- 457 • When $q_{in} > q_c^{clog}$, the flux is higher than the closing threshold, and valves will
 458 stay open, or open if they are closed.
- 459 • When $q_c^{break} < q_{in} < q_c^{clog}$, a closed valve will open because $q_{in} > q_c^{break}$, and
 460 as $q_{in} < q_c^{clog}$, the now-open valve will eventually close. In these conditions, valves
 461 are permanently unsteady, opening and closing in cycles, generating sustained ac-
 462 tivity.

463 In experiments with model porous media, the permeability state (clogged, unclogged or
 464 variable) undergoes similar phase transitions depending on the fluid input rate in the sys-
 465 tem (Jäger et al., 2017; Bianchi et al., 2018).

466 Figure 3 upper panels (a–f) display the cycle of pressure and permeability for a valve,
 467 for three values of q_{in} in the range allowing sustained opening and closing $q_c^{break} < q_{in} <$

468 q_c^{clog} . The closer the input flux q_{in} is to either threshold values, the closer the valve will
 469 be to a permanently closed or open state, as seen in the time series of valve permeabil-
 470 ity (Figure 3b, d, f). For instance in Figure 3a, the flux is just above q_c^{break} . After a rapid
 471 increase of δp when the valve closes, the closed valve is close to an equilibrium and it lets
 472 fluid seep through it as the flux loads it, at a barely superior rate. δp will relatively slowly
 473 reach the breaking threshold δp_c^{break} . When the valve eventually opens, the background
 474 flux is so low that δp quickly drops to the closing point δp_c^{clog} . Overall, the valve spends
 475 most of the time closed, close to opening conditions for q_{in} just above q_c^{break} . Conversely,
 476 if q_{in} is higher, just below q_c^{clog} , the valve takes a much longer time to close when open,
 477 and opens very quickly when closed: it spends more time open overall.

478 This behavior is reflected in the time averaged properties of the valve cycle as a
 479 function of flux, displayed in Figure 3g and h. When close to threshold, the valve rarely
 480 switches states, and produces few events — openings. When q_{in} is far from the critical
 481 values, the valve rapidly loads and relaxes. Because the cycle is faster, the activity rate
 482 is higher. Finally, the proportion of the time the valve is open smoothly transitions from
 483 a mostly closed state to a mostly open state from q_c^{break} to q_c^{clog} , matching the static regime
 484 beyond those values. This progressive permeability evolution from a clogged to an un-
 485 clogged state for increasing values of the hydraulic stressing rate has been observed in
 486 injection experiments in the lab (Candela et al., 2014).

487 Two other parameters shape the valve cycle: valve width w_v and the ratio of closed
 488 to open permeability $\lambda = k_{hi}/k_{lo}$. Valve width governs how quickly fluid can seep through
 489 the valve, and how strong the fluid flux near a valve has to be to impose a given δp across
 490 it. We will show that as two valves of width w_v are close enough, they start behaving
 491 as a macro-valve of larger width. Therefore, the width w_v should be considered the el-
 492 elementary width at which the heterogeneity of permeability is defined, but other scales
 493 of heterogeneity will emerge in systems of many valves where spatial cluster of valves be-
 494 have as macro-valves, and we fix $w_v = 0.01$ for all valves in the rest of the study. As
 495 permeability is the only transport property that is variable in space, the value of λ de-
 496 scribes how quickly fluid pressure diffuses inside a valve relative to outside of it in the
 497 high permeability channel. When this ratio is very high, diffusion within the valve is much
 498 slower than outside the valve, and the effects of the pressure variations outside the valve
 499 will thus dominate the dynamics. In this study, we take $\lambda = k_{hi}/k_{lo} = 20$, for which
 500 closed valves virtually behave as barriers to the fluid diffusion, and the exact value of
 501 this ratio essentially does not influence valve dynamics. Our final goal being to under-
 502 stand how large-scale, complex patterns of valve activation emerge from interactions be-
 503 tween elementary valves, all valves in the rest of the study have fixed parameters (Ta-
 504 ble 1). The main control parameters on valve activity will therefore be the value of the
 505 input flux q_{in} relative to the opening and closing thresholds, and the valve distribution
 506 — their number N_v and position relative to one another in the channel.

507 4 Characterizing source interaction in a two-valve system

508 4.1 Valves interact through pressure transients

509 In order to understand how valves interact through pressure transients and which
 510 parameters control how strong and fast this interaction is, we first design systems with
 511 two valves, and observe how they evolve. Valves are at equal distance from the center
 512 of the channel $x = 0.5$ in normalized length units. The valve width is $w_v = 0.01$, and
 513 the distance between them is d_v , normalized to w_v (Figure 4a).

514 In Figure 4, we describe a simulation in which a system with two valves at a dis-
 515 tance of $d_v = 0.8w_v$ is subjected to a low flux $q_{in} = 0.13$ — close to q_c^{break} , the criti-
 516 cal flux above which closed valves will open. In the permanent regime and independently
 517 of the initial conditions, we observe that the cycles of pressurization and release of both

Temporal behavior of a single valve for different values of the input flux q_{in}

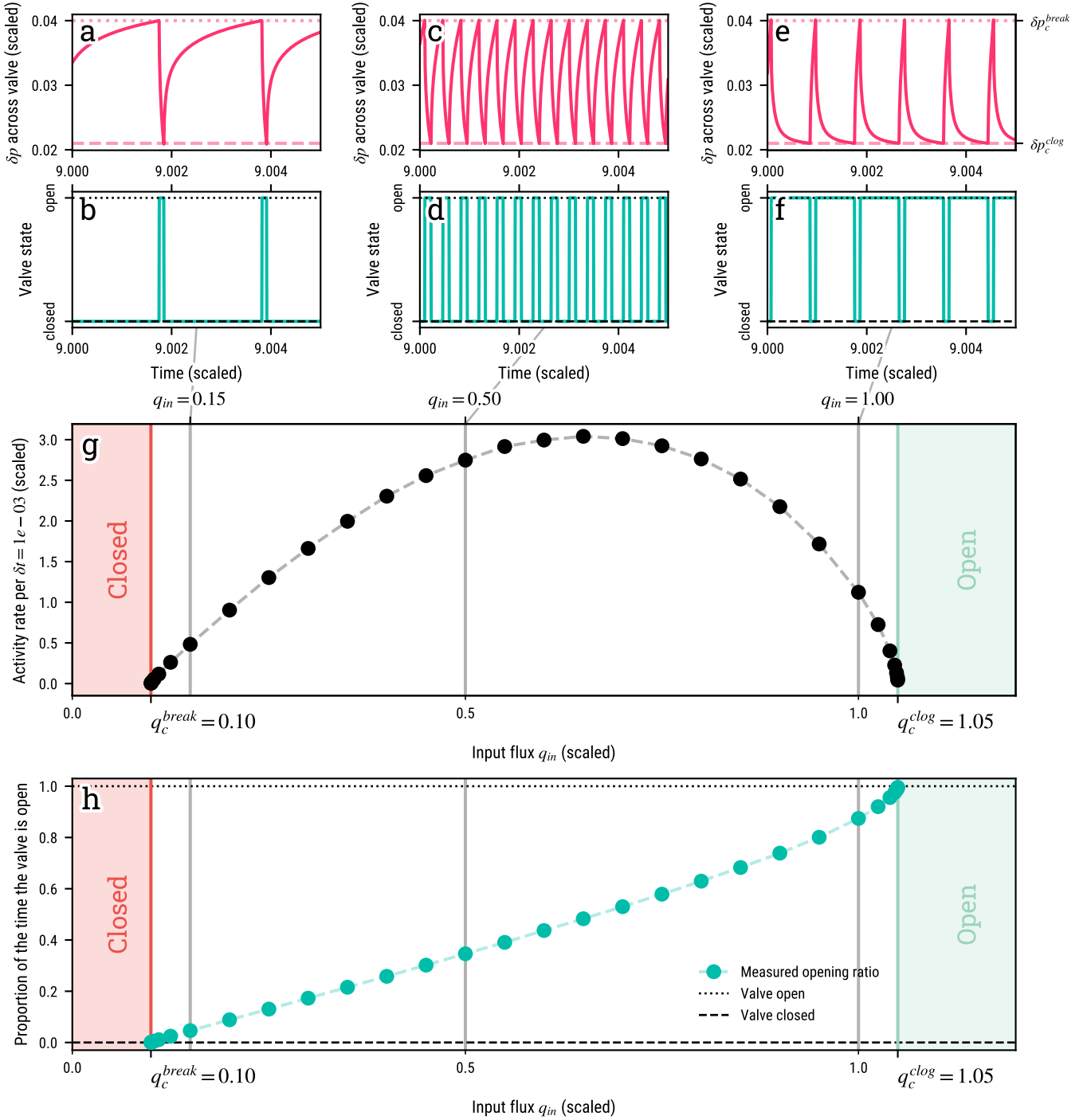


Figure 3. Temporal behavior of a single valve, subjected to different values of the input flux q_{in} , within the range allowing sustained valve activity, $q_c^{break} < q_{in} < q_c^{clog}$. The upper panels (a), (c), (e) display the temporal evolution of fluid pressure difference δp across the valve, while panels (b), (d), (f) show the state of the valve in time, for the same three values of the input flux. See text for a detailed explanation of the regime at each value of q_{in} . (g) Rate of valve openings — model seismic events and (h) proportion of the time a valve is open as a function of q_{in} . In both (g), (h), the activity rate and opening ratio are measured when the behavior of the valve has reached a steady state. For low (resp. high) q_{in} , the valve is closer to threshold, and spends more time in a closed (resp. open) state, close to threshold. Further away from the critical values

Table 1. Valve parameters for all simulations presented in this study

Parameter		Value (scaled)
w_v	Valve width	0.01
k_{hi}	Open valve permeability	1
k_{lo}	Closed valve permeability	0.05
δp_c^{break}	Threshold p difference for opening	0.02
δp_c^{clog}	Threshold p difference for closing	0.0105
q_c^{break}	Flux above which a closed valve will open	0.1
q_c^{clog}	Flux below which an open valve will close	1.05

518 valves (Figure 4b) eventually synchronize, with a short, consistent delay between the first
 519 valve’s opening (downdip valve) and the second valve’s opening (updip valve). The valves
 520 open and close synchronously, and events associated with each opening therefore occur
 521 in a two-event burst, recurring every valve cycle.

522 As we zoom in on the last opening sequence of the simulation (Figure 4c), we ob-
 523 serve that the updip valve is affected with a short delay by the downdip valve’s open-
 524 ing and the flux pulse that it produces. δp across the closed updip valve suddenly rises
 525 due to the fluid influx behind it, and as it is already close to failure, it is sufficient to bring
 526 it to open. It should be noted that in Farge et al. (2021) Section 4.2, we have shown that
 527 this triggering interaction does not necessarily occur from the downdip valve towards the
 528 updip valve. Indeed, the effect of a valve opening updip creates a transiently low pres-
 529 sure in front of the downdip valve, that can trigger its opening.

530 The triggering interaction between valves is therefore carried by the fluid pressure
 531 field in the permeable system. Because it is a diffusive system, the further the trigger-
 532 ing pressure transient has to travel to the neighboring valve, the more the interaction
 533 between the valves is damped and slow. In other words, the distance between valves d_v
 534 should be an essential control on the interaction strength and synchronization.

535 The sensitivity of valves to small variations of pressure around them is also directly
 536 related to their *criticality*: their being close or far to the threshold of δp that will make
 537 them change state — open or close. As shown in the previous section and Figure 3, the
 538 amount of time at the valve spends close to threshold is controlled by the value of the
 539 input flux q_{in} . The closer q_{in} is to critical values q_c^{break} or q_c^{clog} , the closer to thresholds
 540 the valves are on average. In Figure 4b and c, the input flux is $q_{in} = 0.13 \approx q_c^{break} =$
 541 0.1 and it is visible that both v1 and v2 approach δp_c^{break} tangentially. Thus, the closer
 542 q_{in} is to critical values, the stronger the interactions between two valves should be, as
 543 the smallest change of pressure is likely to trigger opening of the valve when it is closed,
 544 and closing of the valve when it is open.

545 4.2 Valve spacing controls activity synchronization

546 In order to characterize the influence of the interval distance d_v on the synchron-
 547 ization of valve activity, we design two-valve systems with various d_v , spanning $d_v =$
 548 0 to $20w_v$. All systems are subjected to a constant flux, and we characterize the event
 549 recurrence timescales when the permanent regime is reached. Various values of flux are
 550 tested for all systems, and in Figure 5, we display the results of this experiment for three
 551 domains of q_{in} , and for the full range of interval distances.

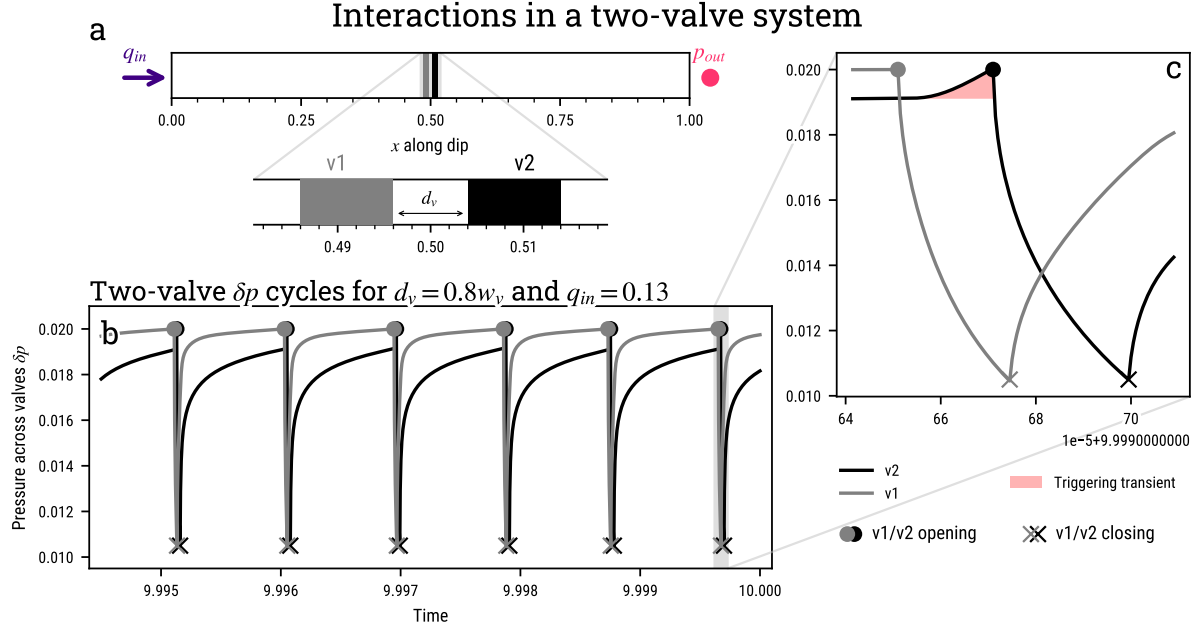


Figure 4. Interactions in a two-valve system. (a) A system with two valves (v1 and v2) spaced by $d_v = 0.008 = 0.8w_v$, subjected to a constant flux $q_{in} = 0.13$, and a constant pressure output $p_{out} = 0$. (b) Cycles of fluid pressure accumulation and release are shown with the time-series of the pressure difference δp across v1 and v2. Closing and opening occur when δp reaches a pre-defined threshold. (c) As v1 opens first and when v2 is critically stressed, the pressure transient that its opening produces (in red) triggers the opening of v2, after a short delay.

552 As the two valves are identical, during the permanent regime of all simulations, the
 553 events occur in repeated sequences of alternating events: a two-event burst (Figure 5).
 554 Two timescales therefore characterize the activity:

- 555 • δt_{intra} the time interval between the first and second opening of the burst
- 556 • δt_{inter} the time interval in between the beginnings of two neighboring bursts, which
 557 can be thought of as the burst recurrence time.

558 In Figure 5b and c, we show the evolution of these two timescales, normalized by δt_0 the
 559 period of the cycle of an isolated, identical valve subjected to the same flux.

560 The first observation is that at large distances ($d_v > 5w_v$, Figure 5b), bursts —
 561 therefore events for each valves — occur with a recurrence corresponding to an isolated
 562 valve: the cycle of either valve is not affected by the other valve. When the distance
 563 between the valves gets shorter, the interaction between valves becomes stronger, produc-
 564 ing two effects on the valves' cycle. (1) In Figure 5c, we observe that for all fluxes, the
 565 closer the valves are (the lower d_v), the shorter δt_{intra} is. As valves get closer, the events
 566 are closer in time, and valves synchronize. (2) In Figure 5b, we observe that as valves
 567 get very close ($d_v < 0.5w_v$ for $q_{in} = 0.11$), δt_{inter} increases for lower and lower d_v —
 568 for all three domains of flux. In other words, the closer the valves, the longer the recur-
 569 rence delay between bursts, and the less frequently valves activate. For such close prox-
 570 imity between valves, the inter-event time is so short that the two valves together can
 571 be considered as a twice-wider *macro-valve*. Interestingly, in Figure 5, we see that for
 572 all fluxes, the *macro-valve* consistently activates with about 4 times the delay of an iso-
 573 lated, elementary valve. We reported the emergence of similar macro-valving behavior

Valve spacing effect on valve-to-valve interaction

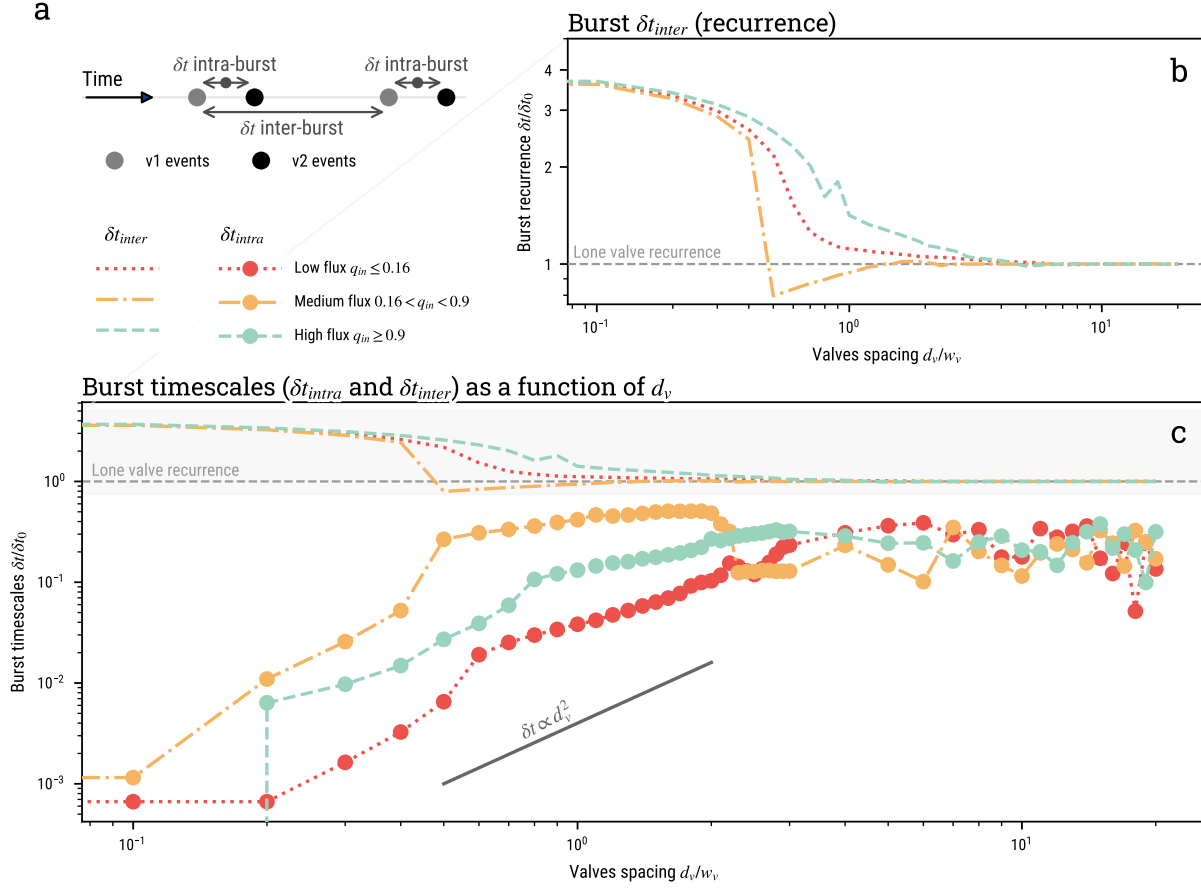


Figure 5. Effect of valve spacing on valve-to-valve interaction. (a) Two timescales describe a two-event burst: δt_{intra} is the delay between events in the burst, and δt_{inter} is the recurrence delay of the burst. In (b) and (c), we observe how δt_{inter} (no markers on the line) and δt_{intra} (circle markers) evolve as a function of valve spacing for low (red, dotted line), intermediate (yellow, dash-dot line) and high (green, dashed line) flux values. Both timescales are normalized by δt_0 , the period of activation of a valve subjected to the same flux. For sufficiently large valve spacing ($d_v > 5w_v$), valves do not interact and act as isolated valves. As valves get closer, events get closer, and the bursts are less frequent.

574 in systems of many strongly-interacting valves in our previous study (Farge et al., 2021,
 575 Section 5.3).

576 A comparison of the curves corresponding to the low, medium and high input flux
 577 ranges in Figure 5b and c allows to assess the effect of the q_{in} on the interaction strength.
 578 In Figure 5b, we see that for low and high q_{in} ranges (red and green curves), which are
 579 closer to critical opening and closing thresholds, the deviation of δt_{inter} from the refer-
 580 ence cycle period (grey line) happens for valve spacings that are wider than for the medium
 581 flux range (yellow curve). Indeed, when subjected to a medium flux range, valves are fur-
 582 ther away from criticality most of the time, and they have to be closer neighbors to in-
 583 teract with a similar intensity as when they are more critical. The same observation can
 584 be made for the delay between events in bursts δt_{intra} : shorter valve spacings are nec-

585 essary in the medium flux range to reach a similarly short delay between events in bursts,
586 compared to the high and low, closer to criticality, flux ranges.

587 Here, we have demonstrated that the interaction between two identical valves are
588 stronger when (1) they are closer together, (2) the flux q_{in} into the channel is close to
589 the thresholds of opening or closing, putting valves in a near-critical state. As interac-
590 tions get stronger, the valves synchronize in time, and their behavior starts resembling
591 that of a larger, less active macro-valve, with different effective permeability and trig-
592 gering thresholds.

593 **5 Emergence and variability of synchronization in complex valve sys-** 594 **tems**

595 **5.1 Control parameters and simulation setup**

596 In reality, the heterogeneous permeability of a fault-zone channel should be com-
597 posed of a complex spatial distribution of valves. In such systems, the synchronization
598 of sources is more complex, and could rely on intricate hydraulic interactions. Based on
599 the results for the two-valve experiments, we investigate how the input flux in the sys-
600 tem and the valve distribution shape interactions in complex N_v -valve systems, and if
601 they are conducive to intermittent, clustered activity, and quasi-periodic bursts. To do
602 so, we run simulations in complex channels with many identical valves, systematically
603 testing how the valve distribution along-dip and values of q_{in} relative to the opening and
604 closing thresholds (q_c^{break} , q_c^{clog}) affect the modeled tremor activity.

605 In the previous section, we have shown that the distance between two valves d_v con-
606 trols the strength of interactions for a given input flux. In a system with $N_v \gg 1$ valves,
607 valves can be close together either because there are many of them in the system, or be-
608 cause of their spatial clustering which results in dense patches separated by less popu-
609 lated regions. In order to test the effect of density and spatial clustering, we design sys-
610 tems where valves are distributed using a Weibull distribution for the inter-valve distance
611 d_v . The probability density function of the distribution is:

$$p(d_v) = \frac{u}{d_0} \left(\frac{d_v}{d_0} \right)^{u-1} \times \exp((-d_v/d_0)^u), \quad (7)$$

612 and its mean

$$\bar{d}_v = d_0 \Gamma \left(1 + \frac{1}{u} \right). \quad (8)$$

613 where d_0 is the scale parameter, u the shape parameter of the distribution, and Γ is the
614 gamma function.

615 The Weibull distribution provides a straightforward parameterization of valve den-
616 sity and spatial clustering in the system, allowing to choose between perfectly regular
617 and highly clustered distributions solely with the choice of the shape parameter u in equa-
618 tion 7. Indeed, when $u \rightarrow +\infty$, the distribution tends toward a Dirac in d_0 — valves
619 are regularly spaced, at a distance of $d_v = d_0$. When $u \rightarrow 0$, the Weibull distribution
620 tends to a power law distribution $p(d_v) \propto d_v^{-1}$. In this case, most valves are spaced with
621 very small d_v , and rarely, a large spacing is drawn, producing a clustered valve distri-
622 bution. Finally, for $u = 1$, the Weibull distribution reduces to an exponential distri-
623 bution $p(d_v) = \exp(-d_v/d_0)/d_0$, of mean $\bar{d}_v = d_0$. In this case, the number of valves
624 in a segment of given length follows a Poisson distribution, and valves are more or less
625 homogeneously distributed across the channel, although at random. As a rule of thumb,
626 this distribution produces clustered point distributions for $u < 1$, and more homoge-
627 neous and regular valve distributions for $u \geq 1$. Finally, the choice of d_0 will allow to
628 specify the average valve distance \bar{d}_v , and therefore number of valves N_v in the system
629 (equation 8).

Parameterizing valve distributions

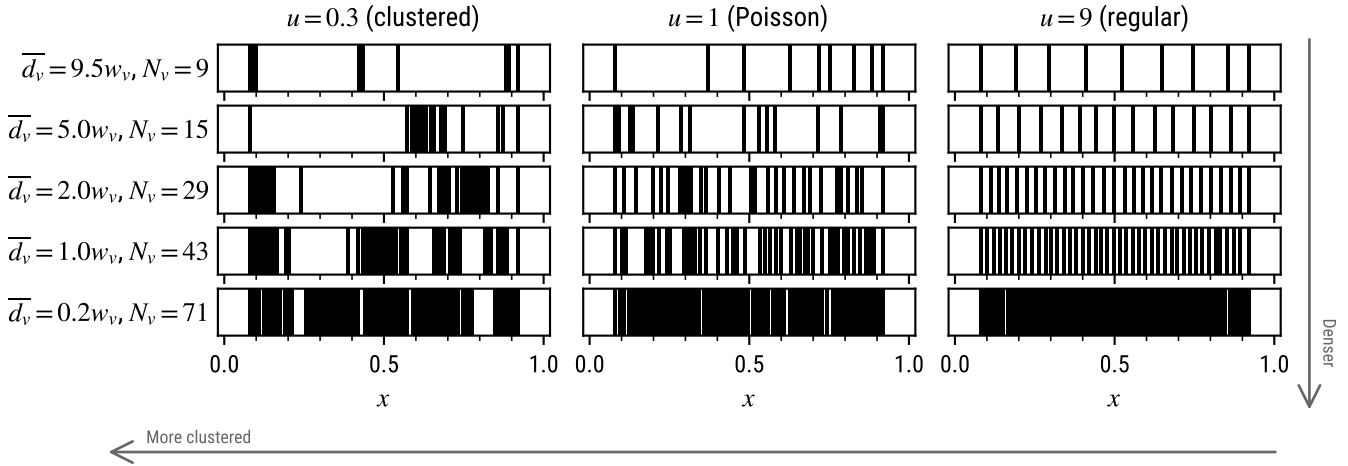


Figure 6. Random realizations of valve distributions for different number of valves N_v and spatial clustering. Valve distributions are generated by drawing valve distances d_v from a Weibull distribution. The valve density, or average valve distance in the domain \bar{d}_v , and therefore the number of valves in the system, are controlled by the theoretical mean of the distribution. The shape parameter u of the Weibull distribution allows to control how clustered or regularly-spaced valves are in space.

630 A valve system is built by first specifying a buffer zone on each sides of the system
 631 to reduce edge effects, common for all distributions, then by randomly drawing inter-valve
 632 distances using the chosen parameters (u and \bar{d}_v), and finally distributing them on the
 633 regular space grid, by simply rounding down the inter-valve distance to the closest discrete
 634 distance possible. We also ensure that the spacing of the last valve to the one before
 635 that is not too far from the target inter-valve distance, so that all valves do not end
 636 up near the input for the most clustered valve distributions. Figure 6 describes the density-
 637 clustering (N_v-u) space of distributions available to us using this technique. Figures S7
 638 and Figures S8 in the Supplementary Information file give a more complete illustration
 639 of this distribution space.

640 We run simulations for distributions described by $N_v = 9-71$ ($\bar{d}_v = 9.5w_v-0.2w_v$,
 641 16 values), $u = 0.2-9$ (8 values, 128 theoretical distributions in total). We randomly
 642 generate 30 distributions for each (N_v, u) , in order to average out the effects of specific
 643 valve arrangements on our results, and obtain statistical significance. In all systems, valves
 644 have identical width, closed permeability and opening/closing δp thresholds (Table 1).
 645 Each system thus defined (3840 total) is subjected to different values of input flux $q_{in} =$
 646 $0.11-1.04$ (11 values), with denser sampling close to the thresholds allowing valve opening
 647 ($q_c^{break} = 0.1$) and closing ($q_c^{log} = 1.05$). In all 42,240 simulations, the output pressure
 648 is kept at $p_{out} = 0$.

649 In addition to pressure, flux and permeability in time and space, we record valve
 650 states in time and space, and build a catalog of valve activations to simulated a seismicity
 651 for each simulation. This catalog is then automatically characterized by computing:

- 652 • the activity rate, measured by the average event count per valve in a given time
653 increment δt ,
- 654 • the extent to which activity occurs in clusters with the clustering index c ($c =$
655 0 events are not clustered at all, $c = 1$ all events occur within clusters),
- 656 • the recurrence timescales of clusters in cases when the activity is clustered in time
657 ($c > 0.25$), measured as the average delay $\text{mean}_k(\Delta T_k)$ between clusters of a same
658 size,
- 659 • and how stable in time the recurrence is, using as an indicator the inverse of the
660 coefficient of variation of the measured delays $\text{mean}_k(\Delta T_k)/\text{std}_k(\Delta T_k)$. When $\text{mean}_k(\Delta T_k)/\text{std}_k(\Delta T_k) >$
661 2 , a simulation is labelled “periodic”.

662 The details of how the latter three measures are computed can be found in Section 2.3.

663 5.2 Control of the input flux on activity synchronization

664 In the previous sections we showed that when the input flux q_{in} is close to the thresh-
665 olds of opening (q_c^{break}) and closing (q_c^{clog}), valves are more sensitive to small changes
666 of pressure. In Section 4, we have shown that this results in strong interactions between
667 valves in two-valve systems subjected to near-threshold q_{in} . With stronger interactions,
668 valve activity tends to synchronize, producing less frequent, more synchronous bursts of
669 events. In Farge et al. (2021), we demonstrated that near-threshold fluxes produce a more
670 clustered seismicity in valve systems with $N_v = 29$ valves, with $u = 1$ (Poissonian valve
671 distribution). Here, we will generalize this analysis to the full spectrum of densities and
672 spatial clustering of valves.

673 We start by focusing on the activity produced in a clustered valve system, $u = 0.3$,
674 with $N_v = 29$ valves ($\bar{d}_v = 2w_v$), for three values of the flux: (a) $q_{in} = 0.13$, near the
675 opening threshold of valves q_c^{break} , valves are mostly closed in average (Farge et al., 2021),
676 (b) $q_{in} = 0.57$, far from thresholds, (c) $q_{in} = 1.02$ near the closing threshold of valves
677 q_c^{clog} . Figure 7 displays the results of the experiment. The first observation is that the
678 results from the two-valve system generalize to this system with $N_v > 2$. In (a) and
679 (c), q_{in} is close to a closing or opening threshold, and activity is intermittent, organized
680 in clusters of events in time, which recur quasi-periodically, whereas when q_{in} is far from
681 both thresholds (in (b)), activity is more continuous, and less clustered. In this system
682 at least, the input flux controls the synchronization of valve activity: the closer to an open-
683 ing or closing threshold it is, the more clustered and periodic the activity seems to be.
684 A second observation is that coherent patterns of activity build over larger distances when
685 the flux is closer to threshold. Indeed, when q_{in} is far from both thresholds, activity is
686 intermittent, but it synchronizes on a much smaller spatial scale than when q_{in} is near-
687 threshold. When valves are more critical, triggering interactions can cascade farther in
688 the system, as most valves are in the same state: close to threshold, and therefore sensi-
689 tive to the opening or closing of their neighbor. When the flux is farther from thresh-
690 old, valves cannot synchronize as well in time and space, as there is less chance that the
691 pressure transient when a valve opens will reach a near-threshold valve. As seen in the
692 two-valve system, the long-range interaction allowed by near-critical fluxes allows large-
693 scale, long-period cycles of activity for large clusters of valves ($0.5 < x < 1$ in Figure 7a.ii).
694 As valves synchronize in space and time, a large-scale valving behavior emerges, favored
695 by valve criticality.

696 Using the full range of our simulations, we extend the analysis to all valve systems,
697 to observe how they respond to values of the flux in between the closing and opening thresh-
698 olds. Figure 8 synthesizes our results. For all valves systems, dense or sparse, clustered
699 or regular, the closer q_{in} is to critical values of the flux, the closer valve systems are to
700 staying closed ($q_{in} \approx q_c^{break}$) or open ($q_{in} \approx q_c^{clog}$). In Figure 8a, we see that valves
701 therefore produce less events just as a result of flux conditions, but also because of valve-
702 to-valve interactions. Interactions between neighboring valves force them into a less fre-

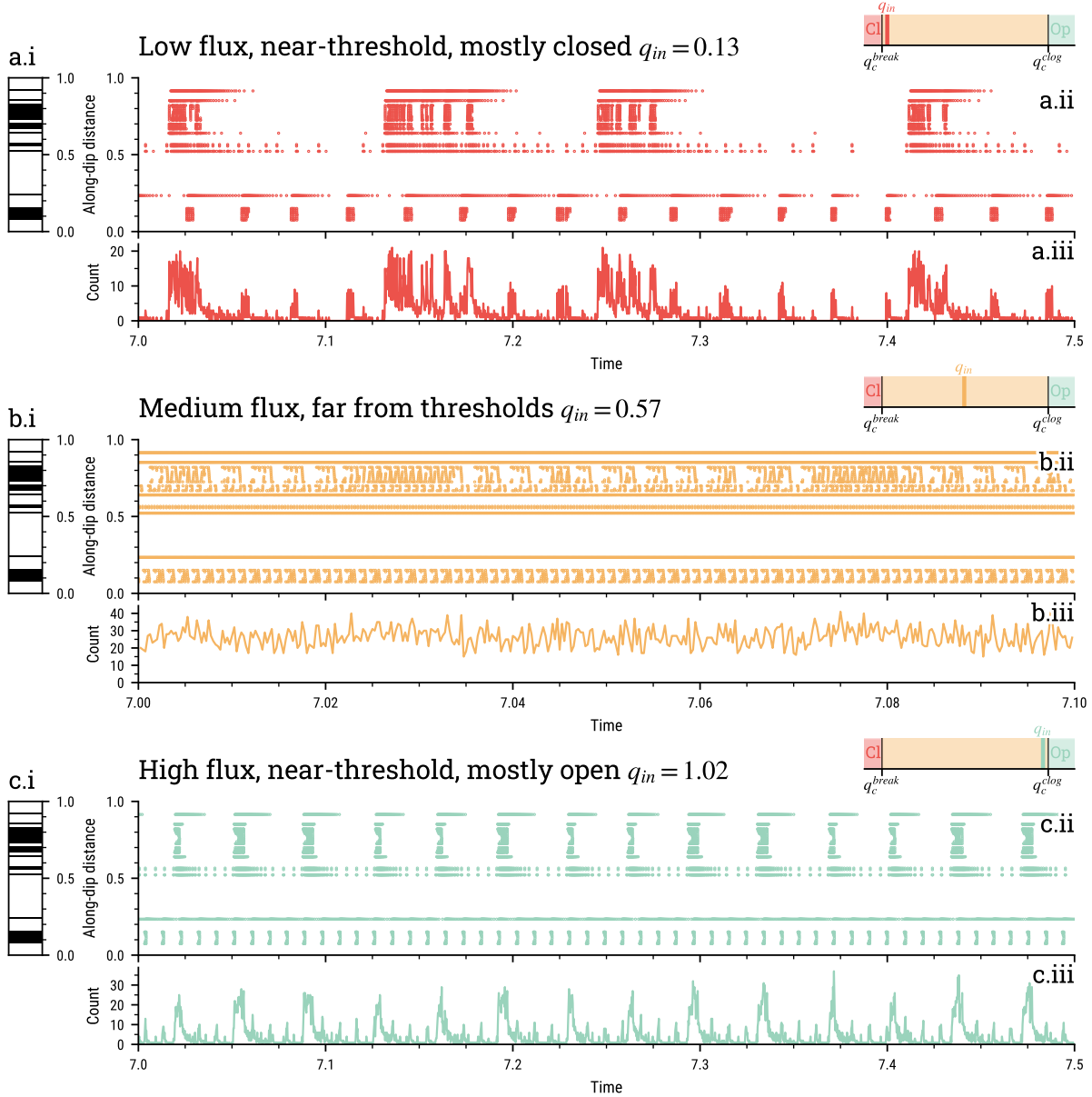


Figure 7. Synthetic tremor activity for three values of the input flux q_{in} (a, b, c) in the same, clustered valve system ($u = 0.3$, $N_v = 29$, $\bar{d}_v = 2w_v$, system b in Figure 9). Panels (a.i), (b.i) and (c.i) represent the valve distributions along the channel. Panels (a.ii), (b.ii) and (c.ii) display the activity along the channel in time, in a time-space diagram where each dot represents the location and time of an opening event. Panels (a.iii), (b.iii) and (c.iii) show the event count (per bin of $\delta t = 2.5e - 4$) time series. The colored panels represent a flux scale, on which q_{in} is represented relative to the opening and closing thresholds. The closer to threshold q_{in} is, the more valves are sensitive to interactions, as they spend more times in a given state. This produces a more synchronized, clustered activity, recurring on long periods. The reader should note the dilated time scale in simulation (b).

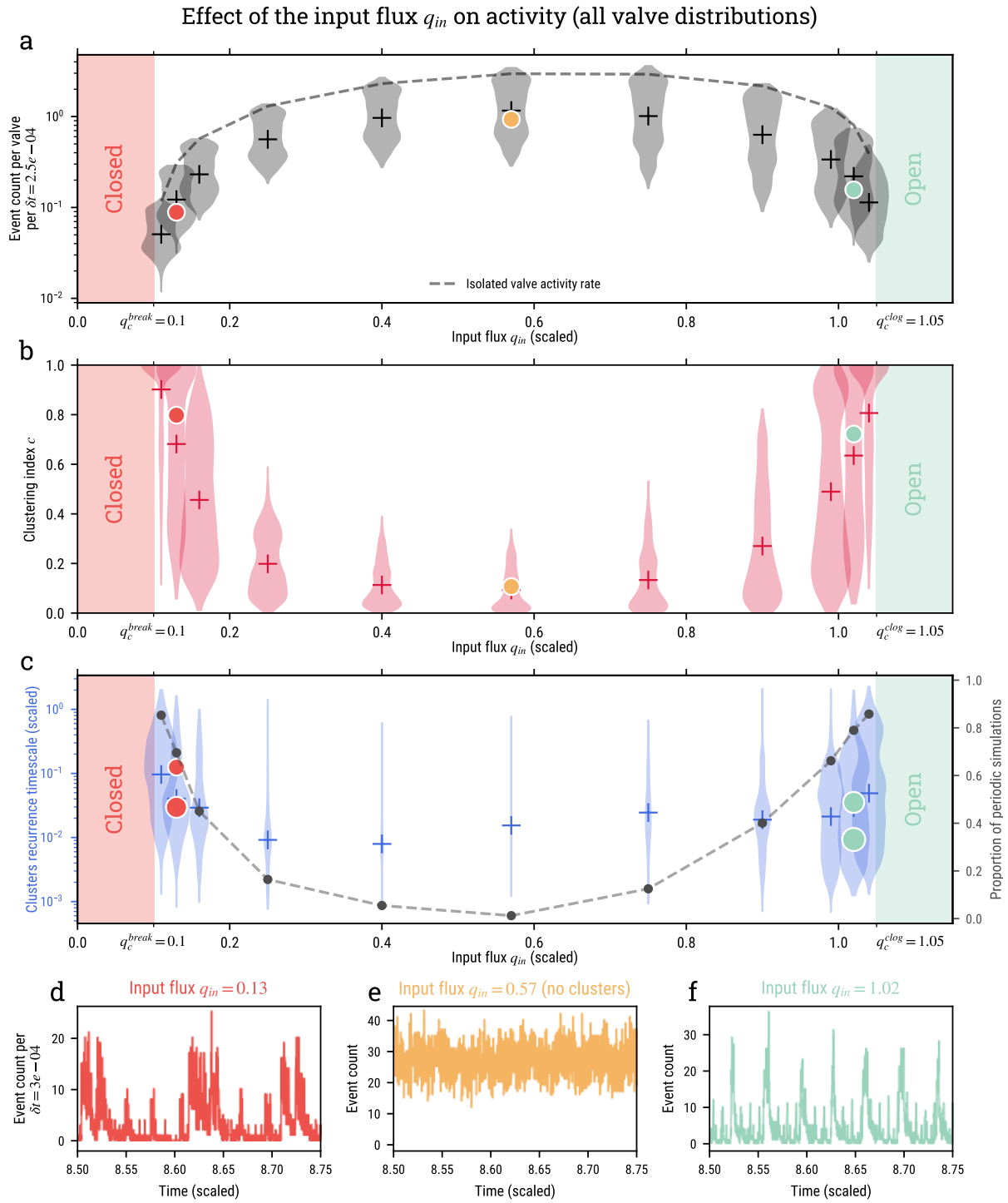


Figure 8 Caption on next page.

Figure 8. Activity rate, temporal clustering and recurrence timescales for different values of the input flux q_{in} , for all valve distributions. (a) Activity rate, computed as the number of events per valve per $\delta t = 2.5e - 4$ (scaled time units). (b) Level of activity clustering measured with the clustering index c , for different values of q_{in} . (c) The average recurrence delay for clusters, as a function of q_{in} . The grey dotted line represents the proportion of periodic simulations (see text for explanation) for each value of q_{in} . In panels (a), (b) and (c), the distribution of measured values for each value of q_{in} is visualized with a violin plot, and the median of all measurements for this q_{in} is represented as a cross. The domains where the flux value prohibits valve activity are shown with red (all valves closed) and green (all valves closed) patches. The colored dots show the clustering and recurrence for the activity in a given system, subjected to three values the input flux. Each corresponding time series of activity is displayed in the bottom panels (d), (e) and (f). The three simulations are performed on a clustered valve distribution ($u = 0.3$) with $N_v = 29$ valves ($\bar{d}_v = 2w_v$), system b displayed in Figures 9b and 11e.

703 quent activation (Figure 5). The closer q_{in} is to thresholds, the more synchronized the
 704 activity gets. Valve activity synchronizes in clusters ($c > 0.5$), and long-range inter-
 705 actions produce macro-valving behavior, which tends to make the activity more periodic,
 706 and with longer periods (Figure 8b and c). As in real systems, periods of burst recur-
 707 rence ($T \sim 10^{-2}$ –1) are orders of magnitude longer than the period of individual valve
 708 cycles ($T \sim 10^{-4}$ – 10^{-3}). When valves in the system experience a flux that is further
 709 from critical conditions, they open and close rapidly, without time to interact and build
 710 synchronicity: activity is high, less clustered, less periodic, with shorter periods.

711 In subduction zones (*e.g.* in Shikoku, Figure 1), most regions exhibit strong tempo-
 712 ral clustering ($c > 0.7$), timescales of burst recurrence several orders of magnitude
 713 longer than individual source recurrence, and coherent activity in space, over scales larger
 714 than the individual source scale. Such conditions are only found in our system for in-
 715 put fluxes into the fault zone that are near-threshold, both low and high. However, it
 716 seems unlikely that the permeable system in the fault zone could stay mostly open. Be-
 717 cause of the high temperature and pressure, ductile deformation of pores and crystal-
 718 lization processes in the pores would rapidly shut most of the pathways (Tarling et al.,
 719 2021), and form pockets of fluid, separated by low-permeability barriers (Gold & Soter,
 720 1985). The near-threshold, low-flux regime ($q_c^{break} < q_{in} < 0.3$) therefore seems to be
 721 the more realistic part of the flux domain. According to our model, in real subduction
 722 zones, a small decrease in flux (between spatial regions or in time) could therefore re-
 723 sult in a monotonic decrease in seismicity, and favor interactions between permeability
 724 valves, thus further lowering seismicity rates, and producing a more clustered, more pe-
 725 riodic activity, synchronizing over larger distances and longer periods. For the rest of this
 726 study, we will thus focus our analysis on low, near-opening-threshold values of the in-
 727 put flux, $q_{in} < 0.3$.

728 5.3 Control of the valve distribution on activity synchronization

729 In Section 4.2, we showed using a simplified system that the interaction between
 730 two valves gets stronger and faster as the distance between them decreases. Those ef-
 731 fects should persist in a more complex system: the closer the valves get in the system,
 732 the more synchronized in time and long-period the activity should be. In order to in-
 733 dependently demonstrate the effect of an increase in valve density (\bar{d}_v and N_v) and spa-
 734 tial clustering (u), we use the activity in three valve systems, (a) a rather homogeneous
 735 system, with $N_v = 29$ valves ($\bar{d}_v = 2w_v$) and a Poissonian distribution of valves ($u =$
 736 1), (b) a system with the same valve density ($N_v = 29$, $\bar{d}_v = 2w_v$) but a more clus-

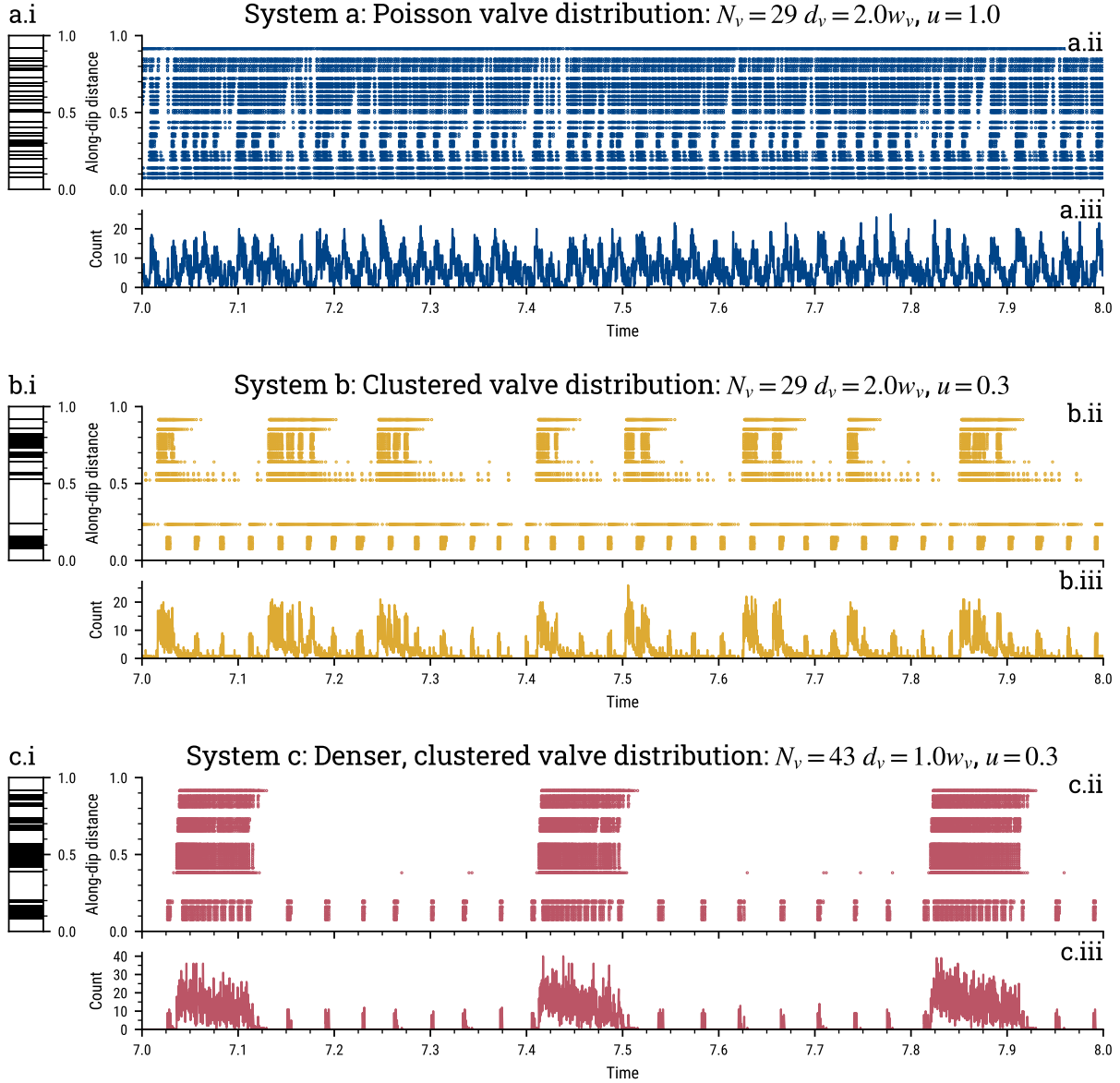


Figure 9. Synthetic tremor activity for three valve systems with different density and clustering (*a*, *b*, *c*). Panels (*a.i*), (*b.i*) and (*c.i*) represent the valve distributions along the channel. Panels (*a.ii*), (*b.ii*) and (*c.ii*) display the activity along the channel in time, in a time-space diagram where each dot represents the location and time of an opening event. Panels (*a.iii*), (*b.iii*) and (*c.iii*) show event count (per bin of $\delta t = 2.5e - 4$) time series. The denser and more clustered the valve system, the more clustered and periodic the activity, and the longer the timescales of recurrence. In other words, the closer the valves get in the system, the more synchronized and long-period the resulting activity seems to become.

737 tered valve distribution $u = 0.3$, and finally (c) a denser system ($N_v = 43$, $\overline{d_v} = 1w_v$),
 738 with the same spatial clustering as in the previous system ($u = 0.3$). All three valve
 739 systems are subjected to a low input flux $q_{in} = 0.13 \approx q_c^{break}$. Figure 9 summarizes
 740 the results.

741 System (a) produces temporally-clustered activity, occurring in bursts, with how-
 742 ever less variability than the other two systems. Indeed, System (b) (Figure 9b.i, b.ii,
 743 b.iii) shares the same number of valves and average valve spacing as System (a) how-
 744 ever the higher spatial clustering of valves creates dense patches of valves in the system,
 745 where valves are locally much closer together than the average inter-valve distance d_v .
 746 The resulting activity is more synchronized, exhibiting clearly separated bursts — of two
 747 sizes, in two different regions of the domain. The burst recurrence is quite variable, but
 748 is obviously longer than for bursts produced in System (a). Finally, System (c) (Figure 9c.i,
 749 c.ii, c.iii) is as spatially clustered as System (b), but with more valves. It is the system
 750 where on average valves are the closest, and also with the most places where valves are
 751 very close locally. The activity it produces is the most clustered of the three: it proceeds
 752 in bursts of two sizes, almost without any activity otherwise. They occur almost peri-
 753 odically, with a more constant, longer period than System (b). Strikingly, the overall ac-
 754 tivity rate in System (c) is lower than in the other two: as in the two-valve system (Sec-
 755 tion 4.2), the longer-recurrence intervals of activity episodes and stronger clustering act
 756 to decrease the overall activity rate of valves in the system.

757 The level of synchronicity of activity increases both as spatial clustering u increases
 758 ((a) to (b)) and as valve density increases ((b) to (c)). This shows that as valves get closer
 759 in the system, their interactions generate stronger interactions, which build clusters of
 760 activations. As elementary valves form spatial clusters in the channel, their collective
 761 behavior builds macro-valves, which produce the bursts of activity seen in system (b)
 762 for instance ($x \approx 0.1$ and $x > 0.5$). The most striking result here is that even though
 763 valve clusters in the channel are far apart, the collective effect of a macro-valve on the
 764 pressure field is such that it builds long-range interaction between valve clusters, which
 765 synchronize valve clusters throughout the channel. This effect occurs in system (c), where
 766 a large-scale valving behavior emerges at the scale of the whole channel, as the four valve
 767 clusters synchronize their activity. In our previous study, we have shown that such cy-
 768 cles of activity are associated with cycles of permeability opening and closing, fluid pres-
 769 sure accumulation and release, similar to the cycle of a single valve (Farge et al., 2021).
 770 The different scales of macro-valving allowed by interactions — cluster of valves (sys-
 771 tem (b), $x < 0.2$), cluster of valve clusters (system (c), full channel) — build increas-
 772 ingly long periodicity of activity, as fluid has to diffuse from the input throughout the
 773 closed system to load all valves to the point of breaking before a collective reopening of
 774 the system.

775 This test is therefore consistent with our hypothesis. The closer the valves get, ei-
 776 ther due to spatial clustering (lower u) or more numerous valves (higher N_v , lower $\overline{d_v}$),
 777 the more synchronized their activity is: they all activate at the same time during bursts,
 778 and are inactive outside of those episodes. In addition, the activity seems to also display
 779 longer recurrence timescales as the valves are closer locally in the system.

780 A simple measure of how many valves are interacting in the system N_v^{int} should
 781 capture how u and N_v both affect the intermittence of activity, and conveniently reduce
 782 the dimension of the problem. We define N_v^{int} as the number of valves that have a neigh-
 783 bor closer than $0.5w_v$, on either side. The value of $d_v < 0.5w_v$ as an interacting dis-
 784 tance is chosen on the basis of the the two-valve experiments described in Section 4: in
 785 Figure 5c, it is visible that valves interact very strongly at distances lower than $d_v =$
 786 $1w_v$ and that this effect is even clearer for $d_v > 0.5w_v$. We choose the lower bound, $d_v <$
 787 $0.5w_v$ for the interacting distance. When the activity characteristics are plotted along
 788 N_v^{int} , we capture the effects of the local proximity of valves in the system, either due to
 789 spatial clustering or overall density. Figure 10 shows systems with different N_v^{int} , show-

790 ing that a similar number of valves can be at interaction distance when the system is dense
 791 and not very clustered, and when it is less dense but with stronger spatially clustered
 792 valves.

793 The results outlined in the previous paragraphs stand for all valve distributions.
 794 In Figure 11, the activity rate, temporal clustering and periodicity are plotted as a func-
 795 tion of the number of interacting valves N_v^{int} , for all valve distributions, subjected to a
 796 low value of flux, close to the closing threshold $q_{in} = 0.13$. The three simulations from 9
 797 are shown as colored dots in panels a, b, and c, and represented again in d, e and f. The
 798 signature of increasing interactions in the system is visible as the number of valves at
 799 interacting distance rises in the system, due to both more clustered or denser distribu-
 800 tion. The closer valves get in the system, the stronger their interactions, and the more
 801 clustered their activity gets ($c > 0.5$, Figure 11b). As they interact strongly, they form
 802 macro-valves, their activity rate drops (Figure 11a), and they activate in clusters with
 803 a more and more periodic behavior (Figure 11c). Finally, as more and larger clusters form
 804 with increasing density and spatial clustering of valves, the activity synchronizes on larger
 805 distances, and becomes periodic on longer timescales (Figure 11c). Strikingly, the vari-
 806 ous space scales of synchronization (macro-valves) seem to be reflected in the detected
 807 periodicities of activity: both short- ($T \approx 3 \times 10^{-2}$) and long-period ($T \approx 3 \times 10^{-1}$)
 808 are detected, corresponding roughly to periodicities of small valve clusters (of width \sim
 809 0.2), and of the full channel — *e.g.* system (c) in Figure 9. Once more, it is notewor-
 810 thy that the periods of activity bursts (5×10^{-3} to 1 scaled time units for most detected
 811 periods) that emerge are orders of magnitude longer than the period of an isolated valve
 812 cycle (8.1×10^{-4} scaled time units for an isolated valve with $q_{in} = 0.13$).

813 The noticeable drop in number of periodic simulations for $N_v^{int} = 45-50$ is an arti-
 814 fact due to the way we design valve systems. In order to test perfectly regular valve
 815 systems, the tested values for N_v jump from 43 to 57. As $N_v^{int} \leq N_v$, systems with $N_v^{int} =$

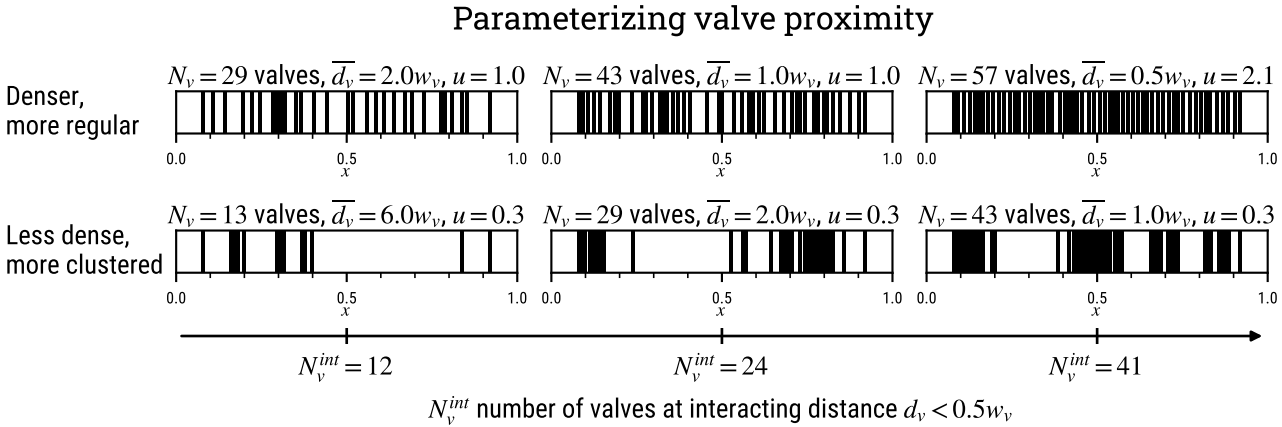


Figure 10. The number of interacting valves N_v^{int} is a measure of how much valves are close from each other in a valve system, either owing to the density of the system (N_v, \bar{d}_v), or to the spatial clustering (u). As valves get closer, they interact more, and N_v^{int} seems to be the best parameter to capture the effects on the style of activity.

Characteristics of activity for different valve systems, $q_{in} = 0.13$

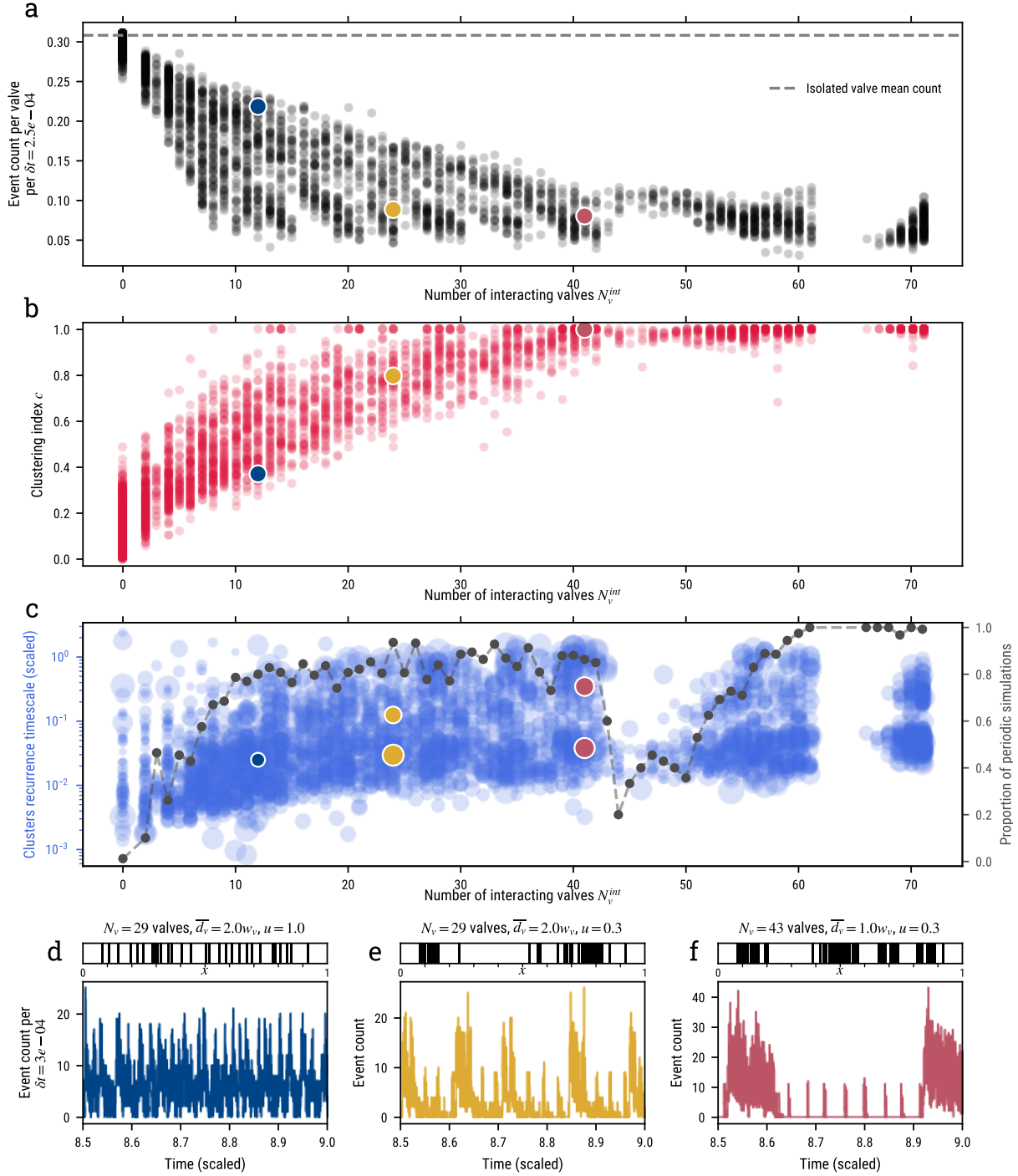


Figure 11: Caption on next page

Figure 11. Intensity, clustering and recurrence timescales of activity for varying levels of interaction in complex valve systems. Results for $q_{in} = 0.13$. (a) Average event count per valve according to the number of interacting valves N_v^{int} . (b) Level of activity clustering measured with the clustering index c , as a function of N_v^{int} . (c) Timescales of cluster recurrence as a function of N_v^{int} . The detected timescales are represented as dots which size scales with the variability of the measured recurrence, estimated as the ratio of the average to the standard deviation of the inter-cluster delays, in the given simulation. The transparency of each data dot is used to convey the density of points in the graph. The dotted line represents the proportion of periodic simulations (see Section 2.3 for details) for each value of N_v^{int} . In panels (a), (b) and (c), the circled, colored dots show the values of clustering and recurrence for three valve systems with increasingly strong valve interactions (same $q_{in} = 0.13$). The three bottom panels (d), (e) and (f) show the corresponding valve distributions (top) and activity (bottom).

816 45–50 are systems which degree of spatial valve clustering is low ($u > 1$), putting valves
 817 far apart. In this case, valve clusters in space are few and small, which results and a less
 818 periodic activity, and lower periodicities — when they emerge.

819 6 Discussion

820 6.1 Linking model parameters and subduction zone hydraulic proper- 821 ties

822 The spatio-temporal patterns of intermittence of tremor in subduction zones gives
 823 the most direct access to minute deformation and hydraulic processes occurring within
 824 or around the subduction interface (*e.g.* Bernaudin & Gueydan, 2018; Cruz-Atienza et
 825 al., 2018; Luo & Liu, 2019). In this work, we propose a simple representation of the hy-
 826 draulic processes in the fault based on elementary permeability-valve processes, in or-
 827 der to investigate the role that hydraulic dynamics may play in shaping the intermittence
 828 of tremor. The main characteristics of tremor we seek to reproduce and understand are
 829 the emergence of the strong temporal clustering of events (Idehara et al., 2014; Frank
 830 et al., 2016; Poiata, Vilotte, Shapiro, Supino, & Obara, 2021), the long, quasi-periodic
 831 recurrence of tremor bursts (Brudzinski & Allen, 2007; Frank et al., 2014; Husker et al.,
 832 2019; Poiata, Vilotte, Shapiro, Supino, & Obara, 2021), and how these two phenomena
 833 vary along-strike in tremor source regions of subduction zones, at scales of tens to hun-
 834 dreds of kilometers (Brudzinski & Allen, 2007; Poiata, Vilotte, Shapiro, Supino, & Obara,
 835 2021). The model we developed reproduces such patterns of seismicity because of inter-
 836 actions between elementary seismic sources through fluid pressure transients in the per-
 837 meable fault interface. We showed that these interactions are the basis of the emergence
 838 of time and space scales of coherent activity much wider than the time and space scale
 839 of activation of a single, isolated source. This feature of our results is valid for a wide
 840 range of the control parameters in our system, and it therefore seems that large-scale,
 841 spatio-temporal patterns of LFE activity in reality could be influenced by slow hydraulic
 842 interaction between sources. In the system we present here, interactions are controlled
 843 by the criticality of valves (q_{in} vs valve thresholds) and valve distribution.

844 We argue that in reality valves should spend most of their times closed, and the
 845 input flux be above, but near their opening threshold q_c^{break} , producing highly intermit-
 846 tent, on-off activity (*cf* Section 5.2). In our system, the distance between q_{in} and q_c^{break}
 847 controls the intermittence of activity. It can change due to changes of (1) q_{in} , (2) valve
 848 breaking threshold δp_c^{break} , and finally of (3) the permeability of the valve when closed
 849 k_{lo} . More generally, those parameters represent (1) a hydraulic stressing rate, (2) a hy-

850 draulic weakness (or strength), and (3) how much the valve translates flow into stress,
 851 a kind of stress-leakage term. The segmentation of tremor intermittence in a real sub-
 852 duction zone could therefore rely on spatial variations of those parameters. The varia-
 853 tions of fluid input is due in part to spatial variations in focusing of the flow in large-
 854 scale permeable channels (Piccoli et al., 2021; Eymold et al., 2021; Angiboust et al., 2014;
 855 Ague, 2014), perhaps dug by past subduction of seamounts (Ide, 2010). The thickness
 856 of the subducting crust, speed and angle of the subduction also controls dehydration rate (Manea
 857 et al., 2013). Variations in temperature can affect how well the fault interface is sealed
 858 from above by silica deposits (Audet & Bürgmann, 2014), and therefore the importance
 859 of sinks and leaking along the fault-zone, which competes with loading rate, inhibiting
 860 valve activity (*e.g.* Halpaap et al., 2019). Finally, the intrinsic properties of the fault zone
 861 govern the strength and permeability of valves, and can strongly be affected by the ge-
 862 ology of the subducting and overriding plates, and local level of damage, controlling both
 863 the availability of pathways for the fluid to circulate and the plasticity of the fault zone
 864 material. Other studies have suggested that local increase in flux and availability of high
 865 fluid pressures might increase the frequency of tremor bursts (McLellan et al., 2022; Wech
 866 & Creager, 2011), but our work stresses that the intensity of q_{in} has to be compared to
 867 the relative contribution of strength and sinks in fluid pressure accumulation in the fault
 868 zone.

869 Indeed, the emergence of temporal clustering and large time and space scales of tremor
 870 activity also relies on the number of interacting sources, which in our description is di-
 871 rectly based on the permeability structure of the fault zone. Our results tend to show
 872 that long-range synchronization and longer timescales are built through the collective
 873 behavior of dense patches of permeability valves in the channel (Section 5.3). Macro-valves
 874 built out of these patches have a strong effect on the pressure field. They are wide, mostly
 875 closed segments of the permeable channel in the fault zone, and by opening all at once,
 876 they generate strong, long-period, long-wavelength variations of fluid pressure, which can
 877 diffuse farther than the transients generated by elementary valve openings, and there-
 878 fore can synchronize the valving and seismic activity of wide parts of the fault zone. In
 879 Section 5.3, we show that for more than $N_v^{int} = 20$ valves at interacting distance, the
 880 produced seismicity is highly temporally clustered, quasi-periodic, on timescales orders
 881 of magnitude longer than single-valve cycles. For the valve widths used here $w_v = 0.01$,
 882 this corresponds to at least 20 % of the system behaving in a valve-like manner, with sig-
 883 nificant spatial clustering of those elementary segments. If it were the case, the observed
 884 patterns of tremor activity could be driven by large-scale, long-period fluid pressure and
 885 permeability transients in the fault zone, built on elementary valving processes. In other
 886 words, N_v^{int} is a rough description of the heterogeneity of permeability of the fault zone.
 887 It is linked with the amount of larger scale irregularities of permeability, which end up
 888 behaving as macro-valves. Ridges, seamounts or fracture zones dominate the kilomet-
 889 ric roughness of the subduction plane, and should define macro structures of permeabil-
 890 ity in the fault. Such structures generate kilometeric-scale heterogeneities of stress, dam-
 891 age, permeability, and mechanical properties of the fault zone. As tremor sources seem
 892 to also be spatially clustered in patches (Rubin & Armbruster, 2013; Ide, 2010; Chestler
 893 & Creager, 2017), the spatially-clustered Weibull distribution ($u < 1$) seems to reason-
 894 ably approximate the physical and observational characteristics of the tremor zone.

895 6.2 Plate topography and tremor segmentation in Shikoku

896 Long-wavelength geophysical observations in subduction zones, of magnetic or gravi-
 897 metric anomalies for instance, reveal that subduction zones are structurally segmented
 898 on a scale of tens to a hundred of kilometers. This segmentation seems to emerge mostly
 899 from the topographic and internal structure of the subducting oceanic plate (Blakely et
 900 al., 2005; Wannamaker et al., 2014; K. Wang & Bilek, 2014; Shillington et al., 2015; Bas-
 901 sett & Watts, 2015), which displays heterogeneous structures — ridges, seamounts, frac-
 902 ture zones — on such a scale. As rough terrain enters the subduction, it modifies stress,

903 damages both the subducting and overriding plate, carries more sediments and water
 904 into the subduction. Those factors can directly affect how seismicity manifests in the rough
 905 segment by modifying the mechanical properties of the fault zone. And indeed, the struc-
 906 tural heterogeneity of the subducting plate often correlates with the spatial variations
 907 of seismicity and tremor along strike in subduction zones, on a very similar scale as the
 908 observed topographic features of the incoming seafloor (Blakely et al., 2005; K. Wang
 909 & Bilek, 2014; Shillington et al., 2015; Bassett & Watts, 2015; Ide, 2010). The topog-
 910 raphy of the incoming plate could directly affect the permeability structure, valving prop-
 911 erties and channeling of the fluid in the fault zone. In the next paragraph, we use the
 912 results of our model to try to link the segmentation of activity in Shikoku with geologic-
 913 scale properties of the plate interface, and interpret how the topography of the subduct-
 914 ing Philippine Sea plate could be the underlying cause of these spatial variations.

915 In Section 2 (Figure 1), we used our novel characterization techniques to propose
 916 a kilometeric-scale segmentation of tremor intermittence in Shikoku. Three segments can
 917 be identified: the first two segments (segment 1 and 2) at each along-strike extremity
 918 ($d < 140$ km, and $d > 190$ km, Figure 1, Figure 12), are characterized by a high level
 919 of clustering and relatively short timescales of recurrence ($T \approx 3$ months). Segment 3
 920 in between is characterized by low, almost exclusively clustered activity, with a longer,
 921 clearer period ($T \approx 6$ months). Interestingly, Ide and Yabe (2014) show that the dom-
 922 inant focal mechanism of very-low-frequency earthquakes (VLFs) are different between
 923 each of those region — a segmentation that our model cannot account for. In Figure 12,
 924 we see that the along-strike extent of those segments and spots of high tremor activity
 925 within them is quite similar to the dimension of seamounts on the seafloor of the Philip-
 926 pine Sea plate, or the ones observed in the accretionary wedge (Yamazaki & Okamura,
 927 1989): about a few tens of kilometers. The alignment of the Kinan seamount chain with
 928 the segmented tremor zone along the convergence direction could indicate that such struc-
 929 tures on the subducting slab, or their lasting effects on the medium as they plow at depth,
 930 are the main factor shaping the segmentation of activity in the Shikoku tremor zone.

931 The segmentation of tremor intermittence in Shikoku can be interpreted as con-
 932 trasts of activity synchronization in time and space, and therefore of interaction strength
 933 between sources. Stronger or weaker source-to-source interactions produce more (seg-
 934 ment 3) or less (segments 1 and 2) clustered, periodic activity, with more or less coher-
 935 ence on large scales of time and space. Our work goes beyond this general interpreta-
 936 tion by showing that such interactions can occur in a dynamically permeable channel
 937 in the fault zone, and that the criticality of sources and their spatial distribution directly
 938 control the interaction strength, and therefore shape the intermittence of activity.

939 The input flux q_{in} partly controls how close valves are to threshold, and therefore
 940 how triggerable they are. If valves are relatively similar for the three segments in Shikoku,
 941 the lower activity, higher temporal clustering and clearer-defined, longer periodicity in
 942 the buffer segment (segment 3, $140 \text{ km} < d < 190 \text{ km}$ along-strike) can be due to a rel-
 943 atively lower metamorphic flux in the region compared to the neighboring regions 1 and
 944 2. The locally lower q_{in} would impose a slower build up of pressure behind the perme-
 945 ability valves, which would spend more time in a closed state, close to their opening thresh-
 946 old. Segment 3 would therefore produce a lower seismicity, and a more clustered, long-
 947 period activity than the end segments 1 and 2, as valves would be closer to threshold.
 948 The same criticality contrast between segments can also arise from a difference in valve
 949 strength, assuming the input fluid flow — and transport properties of the channels —
 950 does not vary significantly along-strike. The valves in the buffer, segment 3, could in-
 951 deed be stronger — higher breaking threshold and/or lower permeability — but under-
 952 going the same fluid input rate. For a constant input flux along-strike, this results in the
 953 same variation of criticality along strike: valves in the buffer region are closer to thresh-
 954 old, producing a more clustered and long-period activity, and valves in the segments 1
 955 and 2 framing it are further from threshold, producing a less clustered, more intense and

956 shorter-period activity. Both these effects can stem from the presence of, or lasting ef-
 957 fects of one or several subducting seamounts (Ide, 2010), that strongly fracture the medium
 958 in the end segments of the tremor zone. The amount of fluid that comes through the in-
 959 terface around the tremor source region would be enhanced by a channeling effect, and
 960 simply by a higher volume of dehydrating crust at depth. In Figure 12, the alignment
 961 of the Kinan seamount chain with the subducting seamount detected by Yamazaki and
 962 Okamura (1989) and the tremor zone could indicate that the chain extends into the sub-
 963 duction, and could result in the tremor activity patterns observed there. Segment 3 that
 964 produces lower, longer-recurrence activity can be a smoother, less damaged region, in
 965 which less fluid is channeled because of a lower channeling effect, and a lower overall per-
 966 meability. In this case, the low flux create a longer recurrence time of periods of open-
 967 ing and activity. Although it might explain the observed activity patterns and it seems
 968 like the most direct interpretation of the intermittence of a system of hydraulic pressure
 969 accumulation and release (McLellan et al., 2022), this interpretation might be at odds
 970 with observations of tidal and dynamic triggering on tremor in patches of highest activ-
 971 ity in the end segments of the zone, and not in the buffer zone (Miyazawa et al., 2008;
 972 Chao et al., 2013; Chao & Obara, 2016; Kurihara et al., 2018). Indeed, if seismicity in
 973 the segments is triggered by minute strains on the interface, it suggests that those seg-
 974 ments might actually be closer to criticality: valves would be more sensitive to the very
 975 small δp changes across them generated by the dynamic strains of tides and teleseismic
 976 waves.

977 It therefore seems that the segmentation could arise from spatial variations of perme-
 978 ability structure, caused by large-scale heterogeneity in the subducting plate topog-
 979 raphy. In a first order analysis, we can assume that the input flux in fault channels, the
 980 background transport properties and the permeability valve characteristics do not sig-
 981 nificantly change across the strike of the tremor zone. A contrast of valve density and
 982 clustering in each segment would therefore explain the segmentation of intermittence.
 983 In this interpretation, we can explain the characteristic activity in the buffer zone, seg-
 984 ment 3, as being due to a higher level of interaction between valves, for instance com-
 985 ing from a higher valve density in this region compared to the neighboring ones. In ge-
 986 ological terms, this would mean a lower overall permeability in segment 3, but a larger
 987 share of the system being dynamic. This could be due to a more homogeneous perme-
 988 able system, perhaps because of a relatively smooth segment of oceanic plate being sub-
 989 ducted in this region. A dense, highly interacting valve network, would produce a remark-
 990 ably synchronized and periodic activity in both time and space and lower overall activ-
 991 ity rate (Figure 9c and 11), and seems that it well describes the seismicity in segment 3.
 992 In this interpretation, the high valve density in the buffer zone would behave as a subduction-
 993 scale valve for the pressure circulation along-strike.

994 6.3 Scope and limitations of model geometry

995 In the previous section, we used our results on space-averaged intermittence of activ-
 996 ity in along-dip channels as representative of the activity in wide segments along the
 997 strike of the subduction. This approach assumes that the behavior of each segment can
 998 be explained by along-dip dynamics of fluid pressure, and that it is isolated from its neigh-
 999 bors, as we neglect the connectivity along-strike, within and between segments. As tremor
 1000 zones often extend much farther along-strike than along-dip (*e.g.* Cascadia and Nankai),
 1001 and as tremor exhibit migrations of activity along-strike, and finally, as hydraulic and
 1002 solid stresses should propagate in all directions, our approach simplifies the problem greatly.

1003 However, we argue that the dynamics in the segments we defined in Shikoku can
 1004 reasonably be collapsed in isolated, along-dip channels for our analysis, which focuses
 1005 on time and space averaged intermittence behavior. Indeed, for the most part, episodes
 1006 of activity mostly span the whole along-strike extension of each segment, and they only
 1007 occasionally communicate.

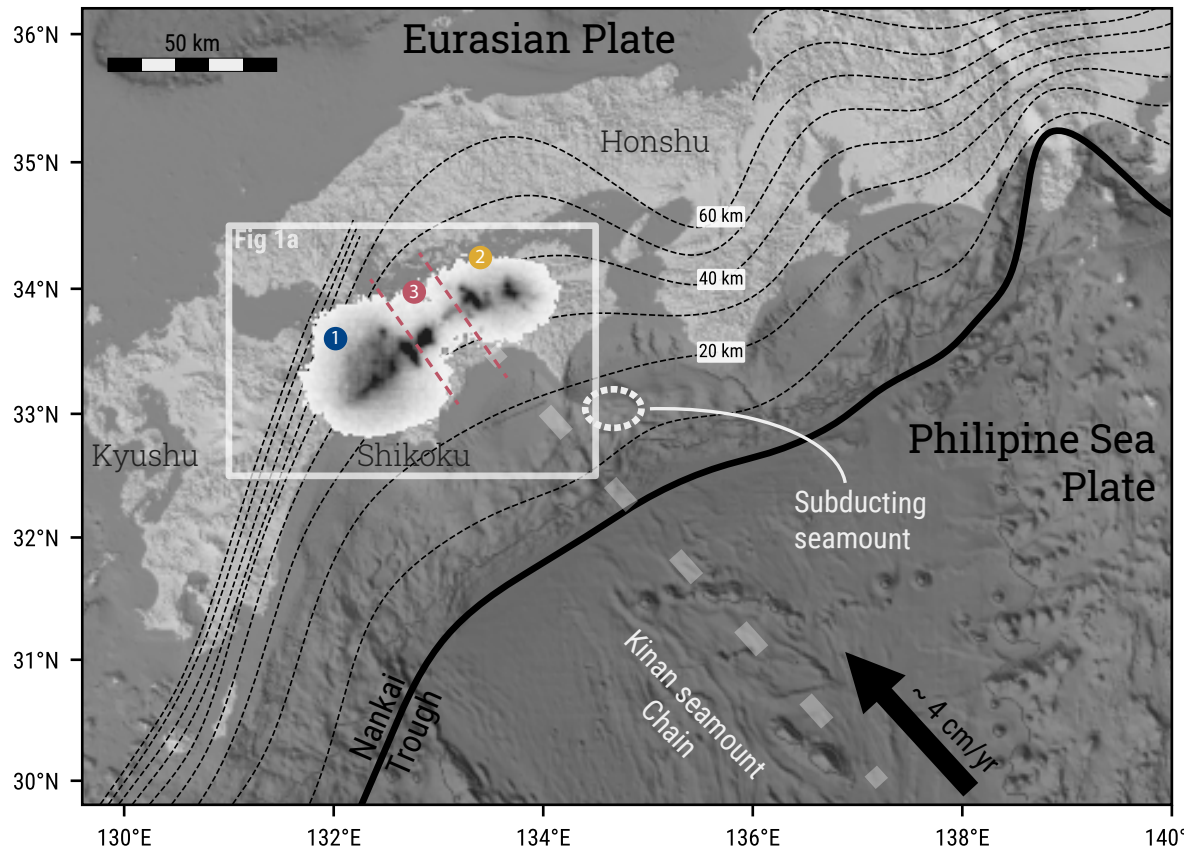


Figure 12. Regional context of the Shikoku subduction and tremor zone. The trench is outlined in thick black line, and the depth contours of the slab are shown in thin dotted black line (model from Iwasaki et al. (2015)). The black arrow and wide dotted line show the direction of relative convergence of the Philippine Sea plate, towards the Eurasian plate (fixed). The extent of the map in Figure 1a is shown with the white box. The three segments defined using the activity are indicated by the numbered circles and dotted lines that divide the tremor zone. We single out rough topographic features on the subducting Philippine Sea plate: the Kinan seamount chain, and a subducting seamount (Yamazaki & Okamura, 1989). Because of their alignment with the tremor zone, and their consistent spatial scale, the presence such topographic features could be responsible for the segmentation of activity witnessed in Shikoku, and displayed as a 2D histogram on the map (*cf* Figure 1 for details).

1008 In our model, generation of tremors is occurring in parts of the faults where the
 1009 fluid pressure is very close to the lithostatic pressure. Therefore, large-scale pressure
 1010 gradient and fluid flow in the tremor generating zone is following the lithostatic gradient —
 1011 from deep metamorphic sources towards shallow sinks. As a consequence the fluid pressure
 1012 gradient and associated fluid flux are dominantly oriented updip with horizontal components
 1013 being on average much weaker. Therefore the tremor — assuming it's associated with
 1014 permeability opening — is mostly associated with upward fluid flow accelerations
 1015 along-dip. Along-strike migrations of activity thus likely track a pulse of

1016 acceleration of updip fluid flow, propagating along the strike of the fault. Such horizon-
 1017 tally propagating pulses can be associated with transient local along-strike fluid pres-
 1018 sure gradients emerging after valve breaking.

1019 This 2D situation can be schematically represented with a series of 1D along-dip
 1020 channel filled with valves and governed by updip pressure gradients. Breaking one valve
 1021 triggers rapid local pressure variations inside the respective channel. These variations
 1022 are then transmitted to a neighbor channel through the along-strike hydraulic connec-
 1023 tivity and eventually trigger closely located valves in this new channel. A cascade of such
 1024 perturbations can propagate near-horizontally and at the same time overall fluid flow
 1025 is still dominantly oriented upwards along-dip.

1026 Further modeling work is needed to understand how the source/sink geometry, the
 1027 two-dimensionnal heterogeneity and anisotropy of permeability, and permeability-opening
 1028 processes could conspire to fuel the complex patterns of migrations of tremor along both
 1029 the strike and dip of the interface.

1030 **6.4 Interactions between fluid circulation and fault slip**

1031 The larger question our work aims to ask is: is fluid pressure and permeability driv-
 1032 ing the dynamics of tremor activity or is fault slip. This model does not intend to faith-
 1033 fully reproduce spatiotemporal patterns of tremor activity, or fluid pressure variations
 1034 in the subduction interface. It is however a framework to reflect about the role of hy-
 1035 draulic stress dynamics with more spatial and temporal complexity. By only looking at
 1036 the dynamics of the hydraulic system, we show that it can reproduce characteristic be-
 1037 havior of tremor and fluid pressure in the fault zone, and that spatial variations of hy-
 1038 draulic properties can lead to variations in tremor intermittence, thereby providing a mech-
 1039 anism that could shape the observed along-strike segmentation of tremor.

1040 It is also clear that shear slip is associated with tremor generation and that the spa-
 1041 tial variations of its dynamics play a role in the segmentation of tremor (Nakajima &
 1042 Hasegawa, 2016; Kano et al., 2018; Cattania & Segall, 2021). Fault slip and tremor ac-
 1043 tivity are linked because their occurrences are to some degree correlated in space and
 1044 time (*e.g.* Rogers, 2003; Hall et al., 2019). At the same time, this correlation is not per-
 1045 fect and detailed observations that the slow slip and tremors are not perfectly co-located
 1046 on the same fault segments (*e.g.* Kostoglodov et al., 2010). Nevertheless, the tremor ac-
 1047 tivity can be used to detect the geodetic signature of small slow slip transients other-
 1048 wise buried in the noise (Frank, Radiguet, et al., 2015). In this interpretation, the tremor
 1049 is generated as brittle asperities rupture when a slip transient occurs on the subduction
 1050 fault (Ando et al., 2010). The seismic characteristics of LFEs — their radiation pattern
 1051 mostly — are also consistent with shear slip on the subduction interface (Ide et al., 2007;
 1052 Royer & Bostock, 2014), although observations interpreted that way are sometimes am-
 1053 biguous, and can sometimes fit a single-force mechanism as well (Wech & Creager, 2007;
 1054 Shapiro et al., 2018; Ohmi & Obara, 2002). The spatio-temporal patterns of tremor could
 1055 therefore be influenced by the dynamics of slip in conditions of near-lithostatic fluid pres-
 1056 sure and heterogeneity of frictional properties of the fault interface (*e.g.* Wech & Crea-
 1057 ger, 2011; Sweet et al., 2019; Luo & Liu, 2019).

1058 The processes of unclogging — or hydrofracture of low permeability barriers — and
 1059 transient fluid pressure that we describe should interact closely with slip on the fault.
 1060 As slip occurs on the fault, be it seismically or aseismically, it generates an extensional
 1061 regime in parts of the fault zone, allowing nearby extension veins to open and pump fluid
 1062 into the fault (Kotowski & Behr, 2019), thus strongly modifying the local permeability
 1063 and fluid pressure in the slipping region. Damage and dilatancy in and around slip also
 1064 create permeability (Tenthorey & Cox, 2006; Mitchell & Faulkner, 2008; Im et al., 2019),
 1065 and can therefore also affect the fluid pressure field.

1066 On the other hand, it is known that high fluid pressure can trigger slip on a fault
 1067 by lowering the effective fault strength. The most plausible cause of an increase of fluid
 1068 pressure is an input of fluid in a partly sealed region. In a homogeneous channel, such
 1069 fluid flow is necessarily associated with a smooth pressure gradient, implying that the
 1070 high fluid pressures that are required for sliding motion are limited to the neighborhood
 1071 of the source. Our study shows how heterogeneous and transient permeability behav-
 1072 ior in the fault could generate high fluid pressures locally and transiently, in wide por-
 1073 tions of the subduction zone. The collective behavior of valves creates a cumulative ef-
 1074 fect on fluid pressure that translates into multi-scale fluid pressure increases and drops,
 1075 that could shape the behavior of fault slip from the source to the subduction scale, thus
 1076 shaping tremor activity, as hinted by the geological record (Angiboust et al., 2015; Taetz
 1077 et al., 2018; Muñoz-Montecinos et al., 2021; Tarling et al., 2021).

1078 We believe the next step in our approach is to understand what scales and observ-
 1079 able behaviors of tremor activity, fluid pressure or slip are specific to a fluid-dominated
 1080 or a deformation-dominated regime, and therefore can help distinguish between them
 1081 in the field. To do so, experimental, theoretical and modeling work is needed to better
 1082 describe the coupling between deformation (induced by pressure and/or slip) and per-
 1083 meability, and what physical parameters control which regime the system is in.

1084 7 Conclusion

1085 The present work should be understood as a simple framework emphasizing the role
 1086 of fluid pressure transients in the occurrence of tectonic tremor in subduction zones. Our
 1087 study is based on the premise that clustering and quasi-periodicity of seismic activity
 1088 should occur when sources synchronize, through interactions. As they synchronize, the
 1089 activity of numerous sources becomes coherent over large scales of space and time. In
 1090 order to measure as explicitly as possible the synchronization of sources, we build novel
 1091 and simple measures of temporal clustering and periodicity in a point-process descrip-
 1092 tion of tremor activity. We propose that the interactions at the origin of the observed
 1093 intermittency of tremor may be mediated by fluid pressure transients in the permeable
 1094 fault zone. In our description, elementary tremor events (LFEs) occur when permeabil-
 1095 ity valves open within the fault zone, stressed by the incoming metamorphic fluid flux
 1096 channeled in the fault zone. We find that how close valves are to their activation thresh-
 1097 old — resulting from a competition between the intensity of the fluid pressure source and
 1098 their mechanical strength — and their spatial distribution in the fault zone both con-
 1099 trol the intermittency of their collective behavior.

1100 In our framework, the highly-clustered, long-period activity of the buffer segment
 1101 in the Shikoku tremor zone develops when densely-packed, highly-interacting valves ac-
 1102 tivate collectively, thus building subduction-scale valving behavior accompanied by large
 1103 bursts of activity. The large timescales of activity, and remarkable spatial coherence of
 1104 the tremor bursts thus emerge from small-scale fluid pressure and permeability cycling
 1105 in the dynamic fault zone, building up through interactions between dynamic segments.
 1106 The segmentation of activity in the tremor zone seems directly linked with the topog-
 1107 raphy of the subducting Philippine Sea plate. While the rough terrains in the extrem-
 1108 ity of the tremor zone should favor less critical valves and a rougher, sparser distribu-
 1109 tion of valves, the smoothness of the slab surface in the buffer segment produces a dy-
 1110 namics adequately represented by a dense valve system. Our model therefore provides
 1111 a simple, physically-based mechanism to describe the influence of hydrological processes
 1112 on shaping tremor patterns in both space and time. More work is needed to refine the
 1113 physical description of hydromechanical processes in this framework, in particular the
 1114 interplay between the slip, the fluid pressure and the permeability. However, we argue
 1115 that including dynamic hydrological processes is crucial to understand tremor and mi-
 1116 croseismicity patterns in general. Beyond the subduction zone setting, we therefore ex-
 1117 pect the permeability-valve framework has a broader reach to interpret how unsteady

1118 fluid circulation processes shape the dynamics of a wide range of geologic plumbing sys-
1119 tems (Journeau et al., 2022; Wech et al., 2020; Ross et al., 2020; Gosselin et al., 2020;
1120 Materna et al., 2019).

1121 **Open Research Section**

1122 The catalogs of tremor and LFE used in this study are available at [https://doi](https://doi.org/10.31905/U0Q9LVHZ)
1123 [.org/10.31905/U0Q9LVHZ](https://doi.org/10.31905/U0Q9LVHZ) for Shikoku, Japan (Poiata, Vilotte, Shapiro, Supino, & Obara,
1124 2021; Poiata, Vilotte, Shapiro, Obara, & Supino, 2021), in the supporting information
1125 of Husker et al. (2019) for Guerrero and Oaxaca (Mexico), and at [https://pnsn.org/](https://pnsn.org/tremor)
1126 [tremor](https://pnsn.org/tremor) for Cascadia (Wech, 2021). The code — still in active development — for the
1127 model is available at <https://github.com/gfarge/PPvalves>.

1128 **Acknowledgments**

1129 This study was supported by the European Research Council under the European Union
1130 Horizon 2020 research and innovation program (Grant Agreement 787399-SEISMAZE).
1131 G. Farge gratefully acknowledges financial support for his research at MIT by the Ful-
1132 bright U.S. Doctoral Program, which is sponsored by the U.S. Department of State and
1133 the French-American Fulbright Commission. The contents of this publication are solely
1134 the responsibility of the author and do not necessarily represent the official views of the
1135 Fulbright Program, the Government of the United States, or the French-American Ful-
1136 bright Commission. Numerical computations were performed on the S-CAPAD/DANTE
1137 platform, IPGP, France. The authors thank S. Rondenay, E. Brodsky, C. Cattania, A.
1138 Schubnel, K. Chanard, two anonymous reviewers and the editor for constructive discus-
1139 sion that led to significant improvement of this manuscript.

1140

References

- 1141 Ague, J. J. (2014, January). 4.6 - Fluid Flow in the Deep Crust. In H. D. Hol-
 1142 land & K. K. Turekian (Eds.), *Treatise on Geochemistry (Second Edition)* (pp.
 1143 203–247). Oxford: Elsevier. doi: 10.1016/B978-0-08-095975-7.00306-5
- 1144 Anderson, R. N., Uyeda, S., & Miyashiro, A. (1976, February). Geophysical and
 1145 Geochemical Constraints at Converging Plate Boundaries—Part I: Dehydration
 1146 in the Downgoing Slab. *Geophysical Journal International*, *44*(2), 333–357.
 1147 doi: 10.1111/j.1365-246X.1976.tb03660.x
- 1148 Ando, R., Nakata, R., & Hori, T. (2010). A slip pulse model with fault heterogene-
 1149 ity for low-frequency earthquakes and tremor along plate interfaces. *Geophys-
 1150 ical Research Letters*, *37*(10). doi: 10.1029/2010GL043056
- 1151 Angiboust, S., Kirsch, J., Oncken, O., Glodny, J., Monié, P., & Rybacki, E. (2015,
 1152 June). Probing the transition between seismically coupled and decoupled
 1153 segments along an ancient subduction interface. *Geochemistry, Geophysics,
 1154 Geosystems*, *16*(6), 1905–1922. doi: 10.1002/2015GC005776
- 1155 Angiboust, S., Pettke, T., De Hoog, J. C. M., Caron, B., & Oncken, O. (2014,
 1156 May). Channelized Fluid Flow and Eclogite-facies Metasomatism along
 1157 the Subduction Shear Zone. *Journal of Petrology*, *55*(5), 883–916. doi:
 1158 10.1093/petrology/egu010
- 1159 Audet, P., & Bürgmann, R. (2014, June). Possible control of subduction zone slow-
 1160 earthquake periodicity by silica enrichment. *Nature*, *510*(7505), 389–392. doi:
 1161 10.1038/nature13391
- 1162 Audet, P., & Kim, Y. (2016, February). Teleseismic constraints on the geological
 1163 environment of deep episodic slow earthquakes in subduction zone forearcs: A
 1164 review. *Tectonophysics*, *670*, 1–15. doi: 10.1016/j.tecto.2016.01.005
- 1165 Bassett, D., & Watts, A. B. (2015, May). Gravity anomalies, crustal structure,
 1166 and seismicity at subduction zones: 1. Seafloor roughness and subducting
 1167 relief: CRUSTAL STRUCTURE AND SEISMICITY: 1. SUBDUCTING
 1168 RELIEF. *Geochemistry, Geophysics, Geosystems*, *16*(5), 1508–1540. doi:
 1169 10.1002/2014GC005684
- 1170 Beaucé, E., Frank, W. B., Paul, A., Campillo, M., & Hilst, R. D. (2019, November).
 1171 Systematic Detection of Clustered Seismicity Beneath the Southwestern Alps.
 1172 *Journal of Geophysical Research: Solid Earth*, *124*(11), 11531–11548. doi:
 1173 10.1029/2019JB018110
- 1174 Beaucé, E., van der Hilst, R. D., & Campillo, M. (2022, September). Microseismic
 1175 Constraints on the Mechanical State of the North Anatolian Fault Zone 13
 1176 Years After the 1999 M7.4 Izmit Earthquake. *Journal of Geophysical Research:
 1177 Solid Earth*, *127*(9). doi: 10.1029/2022JB024416
- 1178 Behr, W. M., & Bürgmann, R. (2021, March). What’s down there? The structures,
 1179 materials and environment of deep-seated slow slip and tremor. *Philosophical
 1180 Transactions of the Royal Society A: Mathematical, Physical and Engineering
 1181 Sciences*, *379*(2193), 20200218. doi: 10.1098/rsta.2020.0218
- 1182 Ben-Zion, Y. (2012, May). Episodic tremor and slip on a frictional inter-
 1183 face with critical zero weakening in elastic solid: NVT-ETS and critical-
 1184 ity. *Geophysical Journal International*, *189*(2), 1159–1168. doi: 10.1111/
 1185 j.1365-246X.2012.05422.x
- 1186 Bernaudin, M., & Gueydan, F. (2018, April). Episodic Tremor and Slip Explained
 1187 by Fluid-Enhanced Microfracturing and Sealing. *Geophysical Research Letters*,
 1188 *45*(8), 3471–3480. doi: 10.1029/2018GL077586
- 1189 Bianchi, F., Thielmann, M., de Arcangelis, L., & Herrmann, H. J. (2018, January).
 1190 Critical Bursts in Filtration. *Physical Review Letters*, *120*(3), 034503. doi: 10
 1191 .1103/PhysRevLett.120.034503
- 1192 Blakely, R. J., Brocher, T. M., & Wells, R. E. (2005). Subduction-zone magnetic
 1193 anomalies and implications for hydrated forearc mantle. *Geology*, *33*(6), 445.
 1194 doi: 10.1130/G21447.1

- 1195 Bostock, M. G., Thomas, A. M., Savard, G., Chuang, L., & Rubin, A. M. (2015).
 1196 Magnitudes and moment-duration scaling of low-frequency earthquakes be-
 1197 neath southern Vancouver Island. *Journal of Geophysical Research: Solid*
 1198 *Earth*, *120*(9), 6329–6350. doi: 10.1002/2015JB012195
- 1199 Brudzinski, M. R., & Allen, R. M. (2007). Segmentation in episodic tremor and slip
 1200 all along Cascadia. *Geology*, *35*(10), 907. doi: 10.1130/G23740A.1
- 1201 Brudzinski, M. R., Hinojosa-Prieto, H. R., Schlanser, K. M., Cabral-Cano, E.,
 1202 Arciniega-Ceballos, A., Diaz-Molina, O., & DeMets, C. (2010, August).
 1203 Nonvolcanic tremor along the Oaxaca segment of the Middle America
 1204 subduction zone. *Journal of Geophysical Research*, *115*, B00A23. doi:
 1205 10.1029/2008JB006061
- 1206 Calvert, A. J., Preston, L. A., & Farahbod, A. M. (2011, August). Sedimentary
 1207 underplating at the Cascadia mantle-wedge corner revealed by seismic imaging.
 1208 *Nature Geoscience*, *4*(8), 545–548. doi: 10.1038/ngeo1195
- 1209 Candela, T., Brodsky, E. E., Marone, C., & Elsworth, D. (2014, April). Labo-
 1210 ratory evidence for particle mobilization as a mechanism for permeability
 1211 enhancement via dynamic stressing. *Earth and Planetary Science Letters*, *392*,
 1212 279–291. doi: 10.1016/j.epsl.2014.02.025
- 1213 Cattania, C., & Segall, P. (2021, April). Precursory Slow Slip and Foreshocks on
 1214 Rough Faults. *Journal of Geophysical Research: Solid Earth*, *126*(4). doi: 10
 1215 .1029/2020JB020430
- 1216 Chao, K., & Obara, K. (2016, January). Triggered tectonic tremor in various types
 1217 of fault systems of Japan following the 2012 M_w 8.6 Sumatra earthquake:
 1218 TRIGGERED TREMOR IN JAPAN. *Journal of Geophysical Research: Solid*
 1219 *Earth*, *121*(1), 170–187. doi: 10.1002/2015JB012566
- 1220 Chao, K., Peng, Z., Gonzalez-Huizar, H., Aiken, C., Enescu, B., Kao, H., ... Mat-
 1221 suzawa, T. (2013, May). A Global Search for Triggered Tremor Following
 1222 the 2011 Mw 9.0 Tohoku Earthquake. *Bulletin of the Seismological Society of*
 1223 *America*, *103*(2B), 1551–1571. doi: 10.1785/0120120171
- 1224 Chestler, S. R., & Creager, K. C. (2017, December). A Model for Low-Frequency
 1225 Earthquake Slip. *Geochemistry, Geophysics, Geosystems*, *18*(12), 4690–4708.
 1226 doi: 10.1002/2017GC007253
- 1227 Cruz-Atienza, V. M., Villafuerte, C., & Bhat, H. S. (2018, December). Rapid tremor
 1228 migration and pore-pressure waves in subduction zones. *Nature Communica-*
 1229 *tions*, *9*(1). doi: 10.1038/s41467-018-05150-3
- 1230 Ester, M., Kriegel, H.-P., Sander, J., & Xu, X. (1996). A Density-Based Algorithm
 1231 for Discovering Clusters in Large Spatial Databases with Noise. *Proceedings of*
 1232 *the 2nd International Conference on Knowledge Discovery and Data mining*,
 1233 226–231.
- 1234 Etheridge, M. A., Wall, V. J., Cox, S. F., & Vernon, R. H. (1984, June). High fluid
 1235 pressures during regional metamorphism and deformation: Implications for
 1236 mass transport and deformation mechanisms. *Journal of Geophysical Research:*
 1237 *Solid Earth*, *89*(B6), 4344–4358. doi: 10.1029/JB089iB06p04344
- 1238 Evans, J. P., Forster, C. B., & Goddard, J. V. (1997, November). Perme-
 1239 ability of fault-related rocks, and implications for hydraulic structure of
 1240 fault zones. *Journal of Structural Geology*, *19*(11), 1393–1404. doi:
 1241 10.1016/S0191-8141(97)00057-6
- 1242 Eymold, W. K., Walsh, T. B., Moortgat, J., Grove, B. S., & Darrah, T. H. (2021,
 1243 April). Constraining fault architecture and fluid flow using crustal noble gases.
 1244 *Applied Geochemistry*, 104954. doi: 10.1016/j.apgeochem.2021.104954
- 1245 Farge, G., Jaupart, C., & Shapiro, N. M. (2021, September). Episodicity and Mi-
 1246 gration of Low Frequency Earthquakes Modeled With Fast Fluid Pressure
 1247 Transients in the Permeable Subduction Interface. *Journal of Geophysical*
 1248 *Research: Solid Earth*, *126*(9). doi: 10.1029/2021JB021894
- 1249 Farge, G., Shapiro, N. M., & Frank, W. B. (2020, August). Moment-Duration Scal-

- ing of Low-Frequency Earthquakes in Guerrero, Mexico. *Journal of Geophysical Research: Solid Earth*, 125(8). doi: 10.1029/2019JB019099
- Frank, W. B., & Brodsky, E. E. (2019, October). Daily measurement of slow slip from low-frequency earthquakes is consistent with ordinary earthquake scaling. *Science Advances*, 5(10), eaaw9386. doi: 10.1126/sciadv.aaw9386
- Frank, W. B., Radiguet, M., Rousset, B., Shapiro, N. M., Husker, A. L., Kostoglodov, V., ... Campillo, M. (2015, April). Uncovering the geodetic signature of silent slip through repeating earthquakes: UNCOVERING SILENT SLIP. *Geophysical Research Letters*, 42(8), 2774–2779. doi: 10.1002/2015GL063685
- Frank, W. B., Shapiro, N. M., Husker, A. L., Kostoglodov, V., Bhat, H. S., & Campillo, M. (2015, March). Along-fault pore-pressure evolution during a slow-slip event in Guerrero, Mexico. *Earth and Planetary Science Letters*, 413, 135–143. doi: 10.1016/j.epsl.2014.12.051
- Frank, W. B., Shapiro, N. M., Husker, A. L., Kostoglodov, V., Gusev, A. A., & Campillo, M. (2016, April). The evolving interaction of low-frequency earthquakes during transient slip. *Science Advances*, 2(4), e1501616. doi: 10.1126/sciadv.1501616
- Frank, W. B., Shapiro, N. M., Husker, A. L., Kostoglodov, V., Romanenko, A., & Campillo, M. (2014, October). Using systematically characterized low-frequency earthquakes as a fault probe in Guerrero, Mexico. *Journal of Geophysical Research: Solid Earth*, 119(10), 7686–7700. doi: 10.1002/2014JB011457
- Fukuda, K., Hatano, T., & Mochizuki, K. (2022, January). Model for tectonic tremors: Enduring events, moment rate spectrum, and moment-duration scaling. *Physical Review E*, 105(1), 014124. doi: 10.1103/PhysRevE.105.014124
- Giger, S. B., Tenthorey, E., Cox, S. F., & Fitz Gerald, J. D. (2007, July). Permeability evolution in quartz fault gouges under hydrothermal conditions. *Journal of Geophysical Research*, 112(B7). doi: 10.1029/2006JB004828
- Goh, K.-I., & Barabasi, A.-L. (2006, October). Burstiness and Memory in Complex Systems. *arXiv:physics/0610233*.
- Gold, T., & Soter, S. (1985). Fluid ascent through the solid lithosphere and its relation to earthquakes. *Pure and Applied Geophysics PAGEOPH*, 122(2-4), 492–530. doi: 10.1007/BF00874614
- Gosselin, J. M., Audet, P., Estève, C., McLellan, M., Mosher, S. G., & Schaeffer, A. J. (2020, January). Seismic evidence for megathrust fault-valve behavior during episodic tremor and slip. *Science Advances*, 6(4), eaay5174. doi: 10.1126/sciadv.aay5174
- Hall, K., Schmidt, D., & Houston, H. (2019, November). Peak Tremor Rates Lead Peak Slip Rates During Propagation of Two Large Slow Earthquakes in Cascadia. *Geochemistry, Geophysics, Geosystems*, 20(11), 4665–4675. doi: 10.1029/2019GC008510
- Halpaap, F., Rondenay, S., Perrin, A., Goes, S., Ottemöller, L., Austrheim, H., ... Eeken, T. (2019, April). Earthquakes track subduction fluids from slab source to mantle wedge sink. *Science Advances*, 5(4), eaav7369. doi: 10.1126/sciadv.aav7369
- Hubbert, M. K., & Willis, D. G. (1957). Mechanics of Hydraulic Fracturing. *Transactions of the AIME*, 210, 153–168.
- Husker, A., Frank, W. B., Gonzalez, G., Avila, L., Kostoglodov, V., & Kazachkina, E. (2019, January). Characteristic Tectonic Tremor Activity Observed Over Multiple Slow Slip Cycles in the Mexican Subduction Zone. *Journal of Geophysical Research: Solid Earth*, 124(1), 599–608. doi: 10.1029/2018JB016517
- Hyndman, R. D., McCrory, P. A., Wech, A., Kao, H., & Ague, J. (2015, June). Cascadia subducting plate fluids channelled to fore-arc mantle corner: ETS and silica deposition. *Journal of Geophysical Research: Solid Earth*, 120(6),

- 1305 4344–4358. doi: 10.1002/2015JB011920
- 1306 Ide, S. (2010, July). Striations, duration, migration and tidal response in deep
1307 tremor. *Nature*, *466*(7304), 356–359. doi: 10.1038/nature09251
- 1308 Ide, S. (2019). Detection of Low-Frequency Earthquakes in Broadband Random
1309 Time Sequences: Are They Independent Events? *Journal of Geophysical Re-*
1310 *search: Solid Earth*, *124*(8), 8611–8625. doi: 10.1029/2019JB017643
- 1311 Ide, S. (2021, December). Empirical Low-Frequency Earthquakes Synthesized From
1312 Tectonic Tremor Records. *Journal of Geophysical Research: Solid Earth*,
1313 *126*(12). doi: 10.1029/2021JB022498
- 1314 Ide, S., & Nomura, S. (2022, December). Forecasting tectonic tremor activity using a
1315 renewal process model. *Progress in Earth and Planetary Science*, *9*(1), 67. doi:
1316 10.1186/s40645-022-00523-1
- 1317 Ide, S., Shelly, D. R., & Beroza, G. C. (2007, February). Mechanism of deep low
1318 frequency earthquakes: Further evidence that deep non-volcanic tremor is
1319 generated by shear slip on the plate interface. *Geophysical Research Letters*,
1320 *34*(3). doi: 10.1029/2006GL028890
- 1321 Ide, S., & Yabe, S. (2014). Universality of slow earthquakes in the very low fre-
1322 quency band. *Geophysical Research Letters*, *41*(8), 2786–2793. doi: 10.1002/
1323 2014GL059712
- 1324 Idehara, K., Yabe, S., & Ide, S. (2014, December). Regional and global variations in
1325 the temporal clustering of tectonic tremor activity. *Earth, Planets and Space*,
1326 *66*(1), 66. doi: 10.1186/1880-5981-66-66
- 1327 Im, K., Elsworth, D., & Wang, C. (2019, May). Cyclic Permeability Evolution Dur-
1328 ing Repose Then Reactivation of Fractures and Faults. *Journal of Geophysical*
1329 *Research: Solid Earth*, *124*(5), 4492–4506. doi: 10.1029/2019JB017309
- 1330 Imanishi, K., Uchide, T., & Takeda, N. (2016). Determination of focal mecha-
1331 nisms of nonvolcanic tremor using S wave polarization data corrected for the
1332 effects of anisotropy. *Geophysical Research Letters*, *43*(2), 611–619. doi:
1333 10.1002/2015GL067249
- 1334 Ito, Y., Obara, K., Shiomi, K., Sekine, S., & Hirose, H. (2007). Slow Earthquakes
1335 Coincident with Episodic Tremors and Slow Slip Events. *Science, New Series*,
1336 *315*(5811), 503–506.
- 1337 Iwasaki, T., Sato, H., Ishiyama, T., Shinohara, M., & Hashima, A. (2015). Fun-
1338 damental structure model of island arcs and subducted plates in and around
1339 Japan. In *AGU Fall Meeting Abstracts* (Vol. 2015, p. T31B-2878).
- 1340 Jäger, R., Mendoza, M., & Herrmann, H. J. (2017, September). The Mechanism
1341 behind Erosive Bursts in Porous Media. *Physical Review Letters*, *119*(12),
1342 124501. doi: 10.1103/PhysRevLett.119.124501
- 1343 Journeau, C., Shapiro, N. M., Seydoux, L., Soubestre, J., Koulakov, I. Y., Jakovlev,
1344 A. V., ... Jaupart, C. (2022, February). Seismic tremor reveals active trans-
1345 crustal magmatic system beneath Kamchatka volcanoes. *Science Advances*,
1346 *8*(5), eabj1571. doi: 10.1126/sciadv.abj1571
- 1347 Kano, M., Kato, A., Ando, R., & Obara, K. (2018, February). Strength of tremor
1348 patches along deep transition zone of a megathrust. *Scientific Reports*, *8*(1),
1349 3655. doi: 10.1038/s41598-018-22048-8
- 1350 Katsumata, A., & Kamaya, N. (2003, January). Low-frequency continuous tremor
1351 around the Moho discontinuity away from volcanoes in the southwest Japan:
1352 DEEP TREMOR IN THE SOUTHWEST JAPAN. *Geophysical Research*
1353 *Letters*, *30*(1), 20-1-20-4. doi: 10.1029/2002GL015981
- 1354 Kostoglodov, V., Husker, A., Shapiro, N. M., Payero, J. S., Campillo, M., Cotte,
1355 N., & Clayton, R. (2010). The 2006 slow slip event and nonvolcanic tremor
1356 in the Mexican subduction zone. *Geophysical Research Letters*, *37*(24). doi:
1357 10.1029/2010GL045424
- 1358 Kotowski, A. J., & Behr, W. M. (2019, August). Length scales and types of hetero-
1359 geneities along the deep subduction interface: Insights from exhumed rocks on

- 1360 Syros Island, Greece. *Geosphere*, 15(4), 1038–1065. doi: 10.1130/GES02037.1
- 1361 Kurihara, R., Obara, K., Takeo, A., & Maeda, T. (2018, April). Migration of Deep
1362 Low-Frequency Tremor Triggered by Teleseismic Earthquakes in the Southwest
1363 Japan Subduction Zone. *Geophysical Research Letters*, 45(8), 3413–3419. doi:
1364 10.1002/2017GL076779
- 1365 Luo, Y., & Liu, Z. (2019). Rate-and-State Model Casts New Insight into Episodic
1366 Tremor and Slow-slip Variability in Cascadia. *Geophysical Research Letters*,
1367 11.
- 1368 Manea, V. C., Manea, M., & Ferrari, L. (2013, December). A geodynamical perspec-
1369 tive on the subduction of Cocos and Rivera plates beneath Mexico and Central
1370 America. *Tectonophysics*, 609, 56–81. doi: 10.1016/j.tecto.2012.12.039
- 1371 Masuda, K., Ide, S., Ohta, K., & Matsuzawa, T. (2020, December). Bridging the gap
1372 between low-frequency and very-low-frequency earthquakes. *Earth, Planets and
1373 Space*, 72(1), 47. doi: 10.1186/s40623-020-01172-8
- 1374 Materna, K., Bartlow, N., Wech, A., Williams, C., & Bürgmann, R. (2019, Novem-
1375 ber). Dynamically Triggered Changes of Plate Interface Coupling in Southern
1376 Cascadia. *Geophysical Research Letters*, 46(22), 12890–12899. doi: 10.1029/
1377 2019GL084395
- 1378 Maury, J., Ide, S., Cruz-Atienza, V. M., & Kostoglodov, V. (2018, February). Spa-
1379 tiotemporal Variations in Slow Earthquakes Along the Mexican Subduction
1380 Zone. *Journal of Geophysical Research: Solid Earth*, 123(2), 1559–1575. doi:
1381 10.1002/2017JB014690
- 1382 McLellan, M., Audet, P., Rosas, J. C., & Currie, C. (2022, December). Margin-wide
1383 variations in slab dehydration in Cascadia and their relationship to slow slip.
1384 *Lithos*, 434–435, 106912. doi: 10.1016/j.lithos.2022.106912
- 1385 Mitchell, T. M., & Faulkner, D. R. (2008, November). Experimental measure-
1386 ments of permeability evolution during triaxial compression of initially intact
1387 crystalline rocks and implications for fluid flow in fault zones. *Journal of
1388 Geophysical Research*, 113(B11), B11412. doi: 10.1029/2008JB005588
- 1389 Miyazawa, M., Brodsky, E. E., & Mori, J. (2008, October). Learning from dynamic
1390 triggering of low-frequency tremor in subduction zones. *Earth, Planets and
1391 Space*, 60(10), e17-e20. doi: 10.1186/BF03352858
- 1392 Muñoz-Montecinos, J., Angiboust, S., Garcia-Casco, A., Glodny, J., & Bebout,
1393 G. (2021, March). Episodic hydrofracturing and large-scale flushing along
1394 deep subduction interfaces: Implications for fluid transfer and carbon recy-
1395 cling (Zagros Orogen, southeastern Iran). *Chemical Geology*, 120173. doi:
1396 10.1016/j.chemgeo.2021.120173
- 1397 Nakajima, J., & Hasegawa, A. (2016, December). Tremor activity inhibited by well-
1398 drained conditions above a megathrust. *Nature Communications*, 7(1), 13863.
1399 doi: 10.1038/ncomms13863
- 1400 Nakajima, J., & Uchida, N. (2018, May). Repeated drainage from megathrusts dur-
1401 ing episodic slow slip. *Nature Geoscience*, 11(5), 351–356. doi: 10.1038/s41561
1402 -018-0090-z
- 1403 Obara, K. (2002, May). Nonvolcanic Deep Tremor Associated with Subduction
1404 in Southwest Japan. *Science*, 296(5573), 1679–1681. doi: 10.1126/science
1405 .1070378
- 1406 Obara, K., Hirose, H., Yamamizu, F., & Kasahara, K. (2004, December). Episodic
1407 slow slip events accompanied by non-volcanic tremors in southwest Japan
1408 subduction zone: EPISODIC SLOW SLIP AND TREMOR IN JAPAN. *Geo-
1409 physical Research Letters*, 31(23). doi: 10.1029/2004GL020848
- 1410 Ohmi, S., & Obara, K. (2002, August). Deep low-frequency earthquakes beneath
1411 the focal region of the Mw 6.7 2000 Western Tottori earthquake: DLF BE-
1412 NEATH THE FOCAL REGION OF THE 2000 WESTERN TOTTORI EQ.
1413 *Geophysical Research Letters*, 29(16), 54-1-54-4. doi: 10.1029/2001GL014469
- 1414 Peacock, S. M., Christensen, N. I., Bostock, M. G., & Audet, P. (2011, May). High

- 1415 pore pressures and porosity at 35 km depth in the Cascadia subduction zone.
 1416 *Geology*, 39(5), 471–474. doi: 10.1130/G31649.1
- 1417 Pedregosa, F., Varoquaux, G., Gramfort, A., Michel, V., Thirion, B., Grisel, O., . . .
 1418 Duchesnay, É. (2011). Scikit-learn: Machine Learning in Python. *Journal of*
 1419 *Machine Learning Research*, 12(85), 2825–2830.
- 1420 Piccoli, F., Ague, J. J., Chu, X., Tian, M., & Brovarone, A. V. (2021, February).
 1421 Field-based evidence for intra-slab high-permeability channel formation at
 1422 eclogite-facies conditions during subduction. *Geochemistry, Geophysics,*
 1423 *Geosystems*. doi: 10.1029/2020GC009520
- 1424 Platt, J. P., Xia, H., & Schmidt, W. L. (2018, December). Rheology and stress
 1425 in subduction zones around the aseismic/seismic transition. *Progress in Earth*
 1426 *and Planetary Science*, 5(1), 24. doi: 10.1186/s40645-018-0183-8
- 1427 Poiata, N., Vilotte, J.-P., Shapiro, N., Obara, K., & Supino, M. (2021, July). *Low-*
 1428 *frequency earthquake catalog for western and central Shikoku, Japan*. doi: 10
 1429 .31905/UOQ9LVHZ
- 1430 Poiata, N., Vilotte, J.-P., Shapiro, N. M., Supino, M., & Obara, K. (2021, Novem-
 1431 ber). Complexity of Deep Low-Frequency Earthquake Activity in Shikoku
 1432 (Japan) Imaged From the Analysis of Continuous Seismic Data. *Journal of*
 1433 *Geophysical Research: Solid Earth*, 126(11). doi: 10.1029/2021JB022138
- 1434 Radiguet, M., Cotton, F., Vergnolle, M., Campillo, M., Walpersdorf, A., Cotte, N.,
 1435 & Kostoglodov, V. (2012). Slow slip events and strain accumulation in the
 1436 Guerrero gap, Mexico. *Journal of Geophysical Research: Solid Earth*, 117(B4).
 1437 doi: 10.1029/2011JB008801
- 1438 Rogers, G. (2003, June). Episodic Tremor and Slip on the Cascadia Subduction
 1439 Zone: The Chatter of Silent Slip. *Science*, 300(5627), 1942–1943. doi: 10.1126/
 1440 science.1084783
- 1441 Ross, Z. E., Cochran, E. S., Trugman, D. T., & Smith, J. D. (2020, June). 3D fault
 1442 architecture controls the dynamism of earthquake swarms. *Science*, 368(6497),
 1443 1357–1361. doi: 10.1126/science.abb0779
- 1444 Royer, A. A., & Bostock, M. G. (2014, September). A comparative study of low fre-
 1445 quency earthquake templates in northern Cascadia. *Earth and Planetary Sci-*
 1446 *ence Letters*, 402, 247–256. doi: 10.1016/j.epsl.2013.08.040
- 1447 Rubin, A. M., & Armbruster, J. G. (2013, December). Imaging slow slip fronts in
 1448 Cascadia with high precision cross-station tremor locations: IMAGING SLOW
 1449 SLIP FRONTS IN CASCADIA. *Geochemistry, Geophysics, Geosystems*,
 1450 14(12), 5371–5392. doi: 10.1002/2013GC005031
- 1451 Rubinstein, J. L., Gomberg, J., Vidale, J. E., Wech, A. G., Kao, H., Creager, K. C.,
 1452 & Rogers, G. (2009, February). Seismic wave triggering of nonvolcanic tremor,
 1453 episodic tremor and slip, and earthquakes on Vancouver Island. *Journal of*
 1454 *Geophysical Research*, 114, B00A01. doi: 10.1029/2008JB005875
- 1455 Sammis, C. G., & Bostock, M. G. (2021). A Granular Jamming Model for Low-
 1456 Frequency Earthquakes. *Journal of Geophysical Research: Solid Earth*, 126(7),
 1457 e2021JB021963. doi: 10.1029/2021JB021963
- 1458 Segall, P., Rubin, A. M., Bradley, A. M., & Rice, J. R. (2010, December). Dilatant
 1459 strengthening as a mechanism for slow slip events. *Journal of Geophysical Re-*
 1460 *search*, 115(B12), B12305. doi: 10.1029/2010JB007449
- 1461 Shapiro, N. M., Campillo, M., Kaminski, E., Vilotte, J.-P., & Jaupart, C. (2018, Oc-
 1462 tober). Low-Frequency Earthquakes and Pore Pressure Transients in Subduc-
 1463 tion Zones. *Geophysical Research Letters*, 45(20), 11,083–11,094. doi: 10.1029/
 1464 2018GL079893
- 1465 Shelly, D. R., Beroza, G. C., & Ide, S. (2007, March). Non-volcanic tremor and
 1466 low-frequency earthquake swarms. *Nature*, 446(7133), 305–307. doi: 10.1038/
 1467 nature05666
- 1468 Shelly, D. R., Beroza, G. C., Ide, S., & Nakamura, S. (2006, July). Low-frequency
 1469 earthquakes in Shikoku, Japan, and their relationship to episodic tremor and

- slip. *Nature*, *442*(7099), 188–191. doi: 10.1038/nature04931
- Shillington, D. J., Bécel, A., Nedimović, M. R., Kuehn, H., Webb, S. C., Abers, G. A., . . . Mattei-Salicrup, G. A. (2015, December). Link between plate fabric, hydration and subduction zone seismicity in Alaska. *Nature Geoscience*, *8*(12), 961–964. doi: 10.1038/ngeo2586
- Sibson, R. (1992, September). Implications of fault-valve behaviour for rupture nucleation and recurrence. *Tectonophysics*, *211*(1-4), 283–293. doi: 10.1016/0040-1951(92)90065-E
- Sibson, R. H. (2017, December). Tensile overpressure compartments on low-angle thrust faults. *Earth, Planets and Space*, *69*(1), 113. doi: 10.1186/s40623-017-0699-y
- Souzy, M., Zuriguel, I., & Marin, A. (2020, June). Transition from clogging to continuous flow in constricted particle suspensions. *Physical Review E*, *101*(6), 060901. doi: 10.1103/PhysRevE.101.060901
- Steinwinder, J., & Beckingham, L. E. (2019, July). Role of Pore and Pore-Throat Distributions in Controlling Permeability in Heterogeneous Mineral Dissolution and Precipitation Scenarios. *Water Resources Research*, *55*(7), 5502–5517. doi: 10.1029/2019WR024793
- Supino, M., Poiata, N., Festa, G., Vilotte, J. P., Satriano, C., & Obara, K. (2020, April). Self-similarity of low-frequency earthquakes. *Scientific Reports*, *10*(1), 1–9. doi: 10.1038/s41598-020-63584-6
- Sweet, J. R., Creager, K. C., Houston, H., & Chestler, S. R. (2019, February). Variations in Cascadia Low-Frequency Earthquake Behavior With Downdip Distance. *Geochemistry, Geophysics, Geosystems*, *20*(2), 1202–1217. doi: 10.1029/2018GC007998
- Taetz, S., John, T., Bröcker, M., Spandler, C., & Stracke, A. (2018, January). Fast intraslab fluid-flow events linked to pulses of high pore fluid pressure at the subducted plate interface. *Earth and Planetary Science Letters*, *482*, 33–43. doi: 10.1016/j.epsl.2017.10.044
- Takei, Y., & Kumazawa, M. (1994, July). Why have the single force and torque been excluded from seismic source models? *Geophysical Journal International*, *118*(1), 20–30. doi: 10.1111/j.1365-246X.1994.tb04672.x
- Tanaka, Y., Suzuki, T., Imanishi, Y., Okubo, S., Zhang, X., Ando, M., . . . Hiraoka, Y. (2018, December). Temporal gravity anomalies observed in the Tokai area and a possible relationship with slow slips. *Earth, Planets and Space*, *70*(1), 25. doi: 10.1186/s40623-018-0797-5
- Tarling, M. S., Smith, S. A., Rooney, J. S., Viti, C., & Gordon, K. C. (2021, June). A common type of mineralogical banding in serpentine crack-seal veins. *Earth and Planetary Science Letters*, *564*, 116930. doi: 10.1016/j.epsl.2021.116930
- Tarling, M. S., Smith, S. A. F., & Scott, J. M. (2019, December). Fluid overpressure from chemical reactions in serpentinite within the source region of deep episodic tremor. *Nature Geoscience*, *12*(12), 1034–1042. doi: 10.1038/s41561-019-0470-z
- Tenthorey, E., & Cox, S. F. (2006). Cohesive strengthening of fault zones during the interseismic period: An experimental study. *Journal of Geophysical Research*, *111*(B9), B09202. doi: 10.1029/2005JB004122
- Ukawa, M., & Ohtake, M. (1987). A monochromatic earthquake suggesting deep-seated magmatic activity beneath the Izu-Oshima Volcano, Japan. *Journal of Geophysical Research*, *92*(B12), 12649. doi: 10.1029/JB092iB12p12649
- Wang, K., & Bilek, S. L. (2014, January). Invited review paper: Fault creep caused by subduction of rough seafloor relief. *Tectonophysics*, *610*, 1–24. doi: 10.1016/j.tecto.2013.11.024
- Wang, T., Zhuang, J., Buckby, J., Obara, K., & Tsuruoka, H. (2018, August). Identifying the Recurrence Patterns of Nonvolcanic Tremors Using a 2-D Hidden Markov Model With Extra Zeros. *Journal of Geophysical Research: Solid*

- 1525 *Earth*. doi: 10.1029/2017JB015360
- 1526 Wannamaker, P. E., Evans, R. L., Bedrosian, P. A., Unsworth, M. J., Maris, V.,
1527 & McGary, R. S. (2014, November). Segmentation of plate coupling, fate of
1528 subduction fluids, and modes of arc magmatism in Cascadia, inferred from
1529 magnetotelluric resistivity. *Geochemistry, Geophysics, Geosystems*, *15*(11),
1530 4230–4253. doi: 10.1002/2014GC005509
- 1531 Warren-Smith, E., Fry, B., Wallace, L., Chon, E., Henrys, S., Sheehan, A., ...
1532 Lebedev, S. (2019, May). Episodic stress and fluid pressure cycling in
1533 subducting oceanic crust during slow slip. *Nature Geoscience*, *1*. doi:
1534 10.1038/s41561-019-0367-x
- 1535 Wech, A. G. (2021). Cataloging Tectonic Tremor Energy Radiation in the Casca-
1536 dia Subduction Zone. *Journal of Geophysical Research: Solid Earth*, *126*(10),
1537 e2021JB022523. doi: 10.1029/2021JB022523
- 1538 Wech, A. G., & Creager, K. C. (2007, November). Cascadia tremor polarization
1539 evidence for plate interface slip. *Geophysical Research Letters*, *34*(22), L22306.
1540 doi: 10.1029/2007GL031167
- 1541 Wech, A. G., & Creager, K. C. (2011, September). A continuum of stress, strength
1542 and slip in the Cascadia subduction zone. *Nature Geoscience*, *4*(9), 624–628.
1543 doi: 10.1038/ngeo1215
- 1544 Wech, A. G., Thelen, W. A., & Thomas, A. M. (2020, May). Deep long-period
1545 earthquakes generated by second boiling beneath Mauna Kea volcano. *Science*,
1546 *368*(6492), 775–779. doi: 10.1126/science.aba4798
- 1547 Yamazaki, T., & Okamura, Y. (1989, March). Subducting seamounts and deformation
1548 of overriding forearc wedges around Japan. *Tectonophysics*, *160*(1), 207–
1549 229. doi: 10.1016/0040-1951(89)90392-2
- 1550 Yasuhara, H., & Elsworth, D. (2008, July). Compaction of a Rock Fracture Moder-
1551 ated by Competing Roles of Stress Corrosion and Pressure Solution. *Pure and*
1552 *Applied Geophysics*, *165*(7), 1289–1306. doi: 10.1007/s00024-008-0356-2